New extended thin-sheet approximation for geodynamic applications—II. Two-dimensional examples

Originally published in:
Gheophysical Journal International 136(3), https://doi.org/10.1046/j.1365-246x.1999.00735.x

Geophys. J. Int. (1999) **136,** 586–608

New extended thin-sheet approximation for geodynamic applications—II. Two-dimensional examples

Sergei E. Medvedev[1,*] and Yuri Yu. Podladchikov[2]

[1] *Institute of Earth Sciences, Uppsala University, Vilavagen* 16, SE-752 36 *Uppsala, Sweden*
[2] *Geologisches Institut, ETH-Zurich, Sonneggstrasse* 5, CH 8092, *Zurich, Switzerland*

Accepted 1998 September 23. Received 1998 September 16; in original form 1998 February 13

SUMMARY

The potential of the new extended thin-sheet approximation (ETSA) has been investigated by application to a representative range of 2-D problems. The system of governing equations presented by Medvedev & Podladchikov (1999) for 3-D modelling was reduced to two dimensions and tested on problems involving one- and two-layer systems of Newtonian viscous materials. The application of ETSA in each case included (1) setting boundary conditions, (2) completion of equations by evaluation of coefficients, (3) comparison of equations with governing equations of existing thin-sheet approximations, and (4) linear analysis of small perturbations and determination of their dominant wavelengths. It is shown that most previous approaches can be derived by simplification of an extended system under specified boundary conditions. Linear analyses compare well with exact analytical solutions over a wide range of wavelengths for modelling isostatic adjustment, Rayleigh–Taylor instabilities and the development of instabilities due to lateral compression and extension. These problems cannot be described by the previous generation of thin-sheet approximations. Our results suggest that the new extended thin-sheet approximation (ETSA) will be a powerful tool for the realistic modelling of complicated 2- and 3-D geodynamic structures.

Key words: compensation depth, crustal deformation, density, perturbation methods, viscosity.

1 INTRODUCTION

Although thin-sheet approximations are useful tools for modelling 3-D lithospheric structures because of their numerical simplicity, there are a number of successful applications in two dimensions (which assume no variation along one of the horizontal coordinates).

We will follow Medvedev & Podladchikov (1999) (hereafter MP99) and divide existing thin-sheet approaches into PS, SS and FP types (Fig. 1). The PS (pure shear) approach assumes negligible vertical gradients in horizontal velocity; the SS (simple shear) approach defines gravitational spreading by equilibration of vertical gradients in horizontal velocities; and the FP (flexing plate) approach recognizes the importance of long-term flexural rigidity of the lithosphere by invoking equilibration of bending moments (Fig. 1).

The equation governing the PS approach (England & McKenzie 1983) can be written for 2-D cases as (our notation)

$$4\,\frac{\partial}{\partial x}\left(\overline{\mu}\,\frac{\partial V_x}{\partial x}\right)=\mathbf{Ar}\,\frac{\partial H^2}{\partial x}\,, \tag{1}$$

where

$$\mathbf{Ar}=\frac{P^*L^*\rho_2\Delta_\rho}{2\mu^*V_x^*\rho_1^2}$$

and $v_x(x, z)=V_x(x)$ (see discussion in Section 6.1 and Tables 1 and 2 for a description of dimensionless variables and characteristic values).

* Present address: Department of Oceanography, Dalhousie University, Halifax, NS, Canada, B3H 4J1. E-mail: sergei@adder.ocean.dal.ca

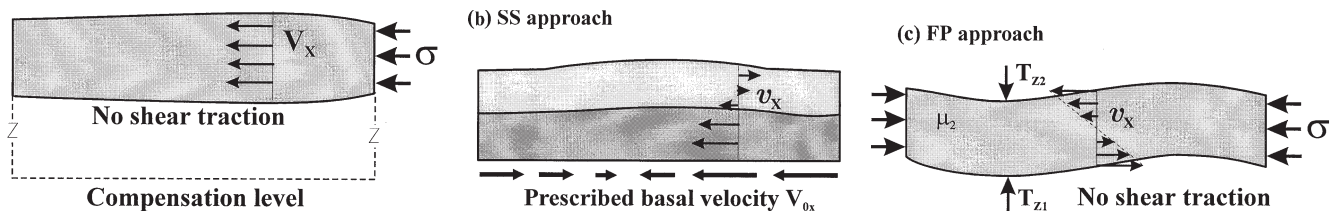

Figure 1. Three main types of thin-sheet approximations are based on viscous rheologies in geodynamic modelling. Their derivations and possible applications are defined by specific boundary conditions. (a) The PS approach is defined by lateral force with zero shear along the lower boundary and Airy isostasy. (b) The SS approach is defined by prescribing a basal velocity field. (c) The dynamics of the FP approach are defined by equilibration of the viscous bending moments. As in the PS approach, no shear is allowed along the external horizontal boundaries. The velocity profiles possible are demonstrated for all cases (the mean velocity of the FP case, describing uniform plate thickening/thinning, is dropped for simplification).

Table 1. Definition of widely used dimensionless variables†.

Variable	Definition	Coordinate dependence	Dimensional scale
a_z	Vertical boundary conditions partitioning coefficient, eq. (14)	–	–
D, E, F, G, J, Q	Coefficients for evaluation of horizontal viscous stress τ_{xx} (eq. 17)	(x, z)	–
$h_1 = S_* - S_1$, $h_2 = S_2 - S_*$	Thickness of rheological layers in two-layer systems	(x)	H^*
h_w, h_*, $\overline{z_c}^{(k)}$	Auxiliary functions of coefficient evaluation (eqs A1–A3)	(x)	–
$M_\mu = \overline{z_c \frac{\mu - \mu_1}{\mu_1}}$	Viscosity heterogeneity momentum in two-layer systems (eq. A3)	(x)	$(H^*)^2$
$M_\rho = \overline{z_c \overline{\rho}}$	Density momentum in vertical force balance (eqs 12, A4)	(x)	$\rho^*(H^*)^2$
R_x, R_z	Dynamic integration functions (eqs 10)	(x)	P^*, $P^* \cdot \varepsilon$
S_1, S_2, S_*	Lower, upper and rheological boundaries of the system	(x)	H^*
$(T_x, T_z)\|_{S_m}$	Vectors of boundary tractions on the external surface S_m, $m = 1, 2$ (eqs 11, 12, 13, 14)	(x)	$(P^*, P^* \cdot \varepsilon)$
t	Time	–	t^*
(V_x, V_z)	Basal velocity vector (kinematic integration functions) (eqs 20)	(x)	(V_x^*, V_z^*)
(v_x, v_z)	Velocity vector	(x, z)	(V_x^*, V_z^*)
w, $z_c = (z - w)$	Reference surface and centred z-coordinate in the integrated vertical force balance (eqs 12, 14)	(x)	H^*
(x, z)	Coordinate system (capital letters denote directions and Z-axis is directed upwards)	–	(L^*, H^*)
α, λ	Growth rate and wavelength of perturbations (eq. 26)	–	$1/t^*$, H^*
$\overline{\Delta T_z}$	Non-lithostatic correction of vertical boundary tractions, (eqs 12, 14)	(x)	P^*
$\Delta_\rho = \rho_2 - \rho_1$, $\Delta_\mu = \mu_2 - \mu_1$	Density and viscosity contrasts in two-layer systems	–	ρ^*, μ^*
$\delta_\mu = \Delta_\mu / \mu_1$	Viscosity heterogeneity in two-layer systems (eq. A3)	–	–
τ_{xx}	Horizontal viscous stress (eq. 15)	(x, z)	P^*

† Non-dimensional variables are used without special notations.

Table 2. Characteristic values.

Value	Definition	Units	Comments
H^*	Vertical length scale	m	$H^* \sim h_1 + h_2$ in two-layer systems
L^*	Horizontal length scale	m	Note that the horizontally oriented parameter λ is scaled by the thickness H^* to emphasize the results
g	Acceleration due to gravity	m s^{-2}	
P^*	Stress	Pa	$P^* = \rho^* g H^*$
t^*	Time	s	$t^* = L^*/V_x^* = H^*/V_z^* = \mu^*/(\rho^* g H^*)$
V_x^*	Horizontal velocity	m s^{-1}	$V_x^* = P^* L^*/\mu^*$
V_z^*	Vertical velocity	m s^{-1}	$V_z^* = P^* H^*/\mu^* = \varepsilon V_x^*$
ε	Small geometry parameter	–	$\varepsilon = H^*/L^* \ll 1$
λ^*	Characteristic wavelength	m	$\alpha(\lambda^*) = \max(\alpha(\lambda))$
μ^*	Viscosity	Pa s	$\mu^* = \mu_1$ in two-layer systems
ρ^*	Density	kg m^{-3}	$\rho^* = \rho_1$ in two-layer systems

The simplicity of the PS approach limits its applications to 2-D problems (Fig. 1a). As part of their complex model, Wdowinski *et al.* (1989) modified the PS approach to model deformations above subduction zones. Neglecting buoyancy forces and adding basal shear traction results in (our notation)

$$4\mu \frac{\partial^2 V_x}{\partial x^2} = -T_x|_{S_1} . \tag{2}$$

This version is supported by asymptotic analysis and allows analytical solutions and agrees well with geophysical observations.

The kinematics of the PS approach are simplified by neglecting vertical variations of horizontal velocity. Since this model applies Airy isostasy (England & McKenzie 1982), the evolution of the thin sheet can be completely described by the evolution of its thickness:

$$\frac{\partial H}{\partial t} = -\frac{\partial}{\partial x}(HV_x) . \tag{3}$$

Potential applications of the SS approach (Fig. 1b) to 2-D models are more general; several studies based on this approach have led to significant developments in the understanding of geodynamic processes. Zanemonetz *et al.* (1976) applied it to modelling the evolution of a two-layer sedimentary basin subjected to vertical movements of its basement. Buck (1991) used a velocity profile based on the SS approach to investigate different modes of lithospheric extension, including core complexes for the first time. Buck & Sokoutis (1994) compared the simplest analytical model of subduction with analogue models to demonstrate zones of horizontal extension above subduction zones. Lobkovsky & Kerchman (1991) included the SS approach in their 'two-level concept of plate tectonics' to describe continental deformations. Bird (1991) and Kaufman & Royden (1994) applied this approach to investigating the influence of lower-crustal flow during deformation of the lithosphere.

Without the principal variations, the governing system of the SS approach is represented in all the works cited as follows:

$$\frac{\partial v_x}{\partial z} = \frac{1}{\mu} \cdot \frac{\partial P}{\partial x} , \qquad \frac{\partial P}{\partial z} = -\rho , \tag{4}$$

which balances the horizontal with the vertical forces. This system allows analytical integration for most cases involving creep rheologies (see e.g. Lobkovsky & Kerchman 1991 for the power-law creep derivation) and direct investigation of thin-sheet kinematics in the form

$$\frac{\partial H}{\partial t} = \mathbf{L}^n[H] - \frac{\partial}{\partial x}(HV_x) , \tag{5}$$

where $\mathbf{L}$ is a non-linear differential operator on H of order $n \geq 2$. The order of this operator and its coefficients depend on the rheology applied. For a single layer with Newtonian viscosity and constant density,

$$\mathbf{L}^n[H] = \frac{\partial}{\partial x}\left(\frac{\rho g H^3}{3\mu} \cdot \frac{\partial H}{\partial x}\right) \tag{6}$$

(after Buck & Sokoutis 1994).

A viscous rheology is one of the main assumptions common to both the PS and SS approaches. By contrast, the FP approach can be based on a variety of rheologies (e.g. Ramberg 1970a; Burov & Diament 1992). The FP approach (Fig. 1c) applied to a viscous rheology is given by the 'general equation for the bending of a thin viscous plate'. Turcotte & Schubert (1982) derived this equation using a step-by-step analogy with the derivation of the elastic plate bending equation. It results in (our notation)

$$\frac{\mu H^3}{3} \frac{\partial^5 S}{\partial^4 x \partial t} + \overline{\sigma} \frac{\partial^2 S}{\partial^2 x} = \overline{T_z} . \tag{7}$$

Solutions of this equation give the vertical displacement, S, of a viscous plate as a function of time (see details in Section 6.1). Application of this equation is limited by the need to invoke large viscosity contrasts between the sheet and its surroundings. The full equations were applied to general cases by e.g. Ramberg (1970a) and Fletcher (1977).

The uses of various existing thin-sheet approximations are limited by a number of restrictions described in MP99. The main aim of this work is to demonstrate that these limitations are not a necessary feature of thin-sheet approximations. MP99 introduced a more accurate approximation (the ETSA) and showed the generality of the ETSA (that is, the possibility of deriving previous approaches by simplification of the ETSA) and its applicability to a wide variety of boundary conditions and rheological profiles (based on creep rheology).

The formulation and final equations of the model are 3-D; however, we employ a 2-D modification of the ETSA here. This simplification renders the governing equations more transparent than the 3-D ETSA model and eases comparison with previous models and exact analytical solutions. Here we apply the 2-D reduction of the ETSA to problems with boundary conditions related to previous thin-sheet investigations (Fig. 1) and rheological profiles based on Newtonian viscous materials (Fig. 2).

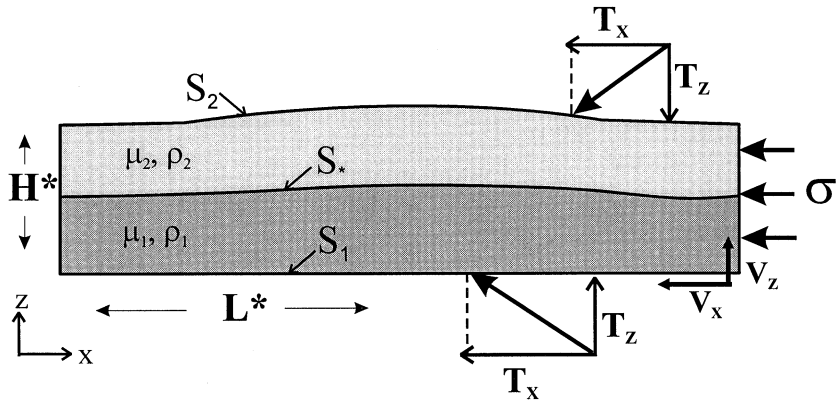

Figure 2. A general view of a thin sheet defined by condition $L^* \gg H^*$. The possibility of introducing layered systems is illustrated by the internal rheological boundary S_*. The rheology is described by Newtonian viscosities and densities which are constant within each layer. The balance with external conditions is described by boundary tractions T (applied on external boundaries S_1 and S_2), basal velocity V and lateral stress σ.

Note that we only use non-dimensional values. Table 3 demonstrates a method to obtain dimensional values using Tables 2 and 1.

2 SYSTEM OF 2-D EQUATIONS FOR THE ETSA

The asymptotic investigations of Stokes' equations presented in MP99 result in approximate profiles of pressure and vertical shear stress, which can be rewritten for the 2-D case as

$$P(x, z) \cong - R_z - \tau_{xx} - \int_{S_1}^{z} \rho dz' , \tag{8}$$

$$\tau_{xz}(x, z) \cong R_x + \int_{S_1}^{z} \frac{\partial}{\partial x} (P - \tau_{xx}) dz' , \tag{9}$$

where R_z and R_x represent the first set of dynamic key functions,

$$\begin{aligned} R_z(x) &= (\tau_{zz} - P)|_{S_1} , \\ R_x(x) &= \tau_{iz}|_{S_1} \end{aligned} \tag{10}$$

(see Tables 1 and 3 for notation). The inaccurate profiles in eqs (8) and (9) are verified by the exact equilibration of the integrated force balance. This results in the system of equations governing the ETSA. Restricting this system to two dimensions (eqs 26 and 27 of MP99) results in the following form:

$$2 \frac{\partial \overline{\tau_{xx}}}{\partial x} + \frac{\partial}{\partial x} (R_z H + \overline{\overline{\rho}}) + \overline{T_x} = 0 , \tag{11}$$

$$\frac{\partial^2}{\partial x^2} [2\overline{z_c \tau_{xx}} + \overline{M_\rho} + R_z \overline{z_c}] + \frac{\partial}{\partial x} \left[(2\overline{\tau_{xx}} + R_z H + \overline{\overline{\rho}}) \frac{\partial w}{\partial x} \right] + \frac{\partial}{\partial x} (\overline{z_c T_x}) + \overline{\Delta T_z} = 0 . \tag{12}$$

Here $\overline{T_x}$ and $\overline{\Delta T_z}$ represent the second set of dynamic key functions, those which refer to the sum of the external tractions acting along the horizontal boundaries S_1 and S_2. The relationship between the key dynamic functions and the full boundary tractions are

Table 3. Designation.

Attribute	Definition	Examples
	Superscripts	
*	Characteristic value (Table 1)	
d	Dimensional value	Using Table 1, for any function: $F^d = F \cdot$ (Dim. scale)
	Special designation	
Vertical bar with one subscript	Function value on selected z level	$v|_{S_1} = v(x, S_1(x))$
Vertical bar with two limits	Difference operator between its upper and lower limits	$(z_c \cdot \tau_{xx})|_{S_1}^{S_2} = (S_2 - w)\tau_{xx}|_{S_2} - (S_1 - w)\tau_{xx})|_{S_1}$
Overbar (1)	For continuous functions: Z integrating through the system (note that there is no normalizing by H)	$\overline{P}(x, y) = \int_{S_1}^{S_2} P(x, z) dz$, $\overline{z \cdot \overline{\rho}} = \int_{S_1}^{S_2} z \cdot \left(\int_{S_1}^{z} \rho, dz' \right) dz$
Overbar (2)	For discrete functions: sum values of the function at upper and lower external boundaries	$\overline{T_x} = T_x|_{S_1} + T_x|_{S_2}$, $\overline{z \cdot T_x} = S_1 T_x|_{S_1} + S_2 T_x|_{S_2}$

defined by

$$T_x|_{S_1} = -R_x + (2\tau_{xx}|_{S_1} + R_z)\,\frac{\partial S_1}{\partial x}\,,$$
$$T_x|_{S_2} = \overline{T_x} - T_x|_{S_1}\,, \tag{13}$$
$$T_z|_{S_1} = -R_z - \varepsilon^2(a_z - 1)\overline{\Delta T_z}\,,$$
$$T_z|_{S_2} = R_z + \overline{\rho} + \varepsilon^2 a_z \overline{\Delta T_z}\,, \tag{14}$$
$$\overline{\Delta T_z} = \varepsilon^{-2}(\overline{T_z} - \overline{\rho})\,.$$

The last equilibration in eqs (14) illustrates the use of $\overline{\Delta T_z}$ to correct the lithostatic model to the full vertical force balance. The partitioning coefficient, a_z, is a free parameter in the ETSA. It illustrates the relation between the approximate vertical stress profile eq. (8) and the exact boundary stresses in eqs (14). Setting $a_z = 1$ (or $a_z = 0$) results in satisfying the bottom (or upper) boundary condition exactly by the approximate profile expressed in eq. (8). We will use examples to explore how the results depend on this parameter.

The application of creep rheology results in the following approximation of horizontal viscous stress integrated over depth:

$$\overline{\tau_{xx}} = 2\left[(\overline{\mu} - 4\overline{G_{xx}} + \overline{F_{xx}})\,\frac{\partial V_x}{\partial x} - (4\overline{G_{*x}} + 4\overline{G_{x*}} - 2\overline{F_{x*}})\,\frac{\partial^2 V_x}{\partial x^2} - (4\overline{G_{**}} - \overline{F_{**}})\,\frac{\partial^3 V_x}{\partial x^3}\right.$$
$$\left. + (\overline{D_x} - \overline{\tilde{D}_{xxx}})R_x + (\overline{D_*} - 3\overline{\tilde{D}_{*xx}})\,\frac{\partial R_x}{\partial x} - 3\overline{\tilde{D}_{**x}}\,\frac{\partial^2 R_x}{\partial x^2} - \overline{\tilde{D}_{***}}\,\frac{\partial^3 R_x}{\partial x^3} + \overline{J_x}\,\frac{\partial V_z}{\partial x} - \overline{J_*}\,\frac{\partial^2 V_z}{\partial x^2} - \overline{E_x}\,\frac{\partial R_z}{\partial x} - \overline{E_*}\,\frac{\partial^2 R_z}{\partial x^2} - \overline{Q_{xx}}\right]. \tag{15}$$

A similar expression describes the averaged moment of the horizontal viscous stress τ_{xx}:

$$\overline{z_c \cdot \tau_{xx}} = 2\left[(\overline{z_c \cdot \mu} - 4\overline{z_c \cdot G_{xx}} + \overline{z_c \cdot F_{xx}})\,\frac{\partial V_x}{\partial x} - \ldots(\text{other terms})\right]. \tag{16}$$

Here the coefficients are defined by

$$D_x = \varepsilon^2 \cdot \mu\,\frac{\partial}{\partial x}\left(\int_{S_1}^{z}\frac{1}{\mu}\,dz'\right),$$
$$\tilde{D}_{xxx} = \varepsilon^4 \cdot \mu\,\frac{\partial}{\partial x}\left(\int_{S_1}^{z}\left(\frac{\partial}{\partial x}\int_{S_1}^{z'}\frac{\partial}{\partial x}\left(\int_{S_1}^{z''}\frac{1}{\mu}\,dz'''\right)dz''\right)dz'\right),$$
$$E_x = \varepsilon^2 \cdot \mu\,\frac{\partial}{\partial x}\left(\int_{S_1}^{z}\frac{(z' - S_1)}{\mu}\,dz'\right),$$
$$F_{xx} = \varepsilon^2 \cdot \mu\,\frac{\partial^2}{\partial x^2}\left(\frac{(z - S_1)^2}{2}\right), \tag{17}$$
$$G_{xx} = \varepsilon^2 \cdot \mu\,\frac{\partial}{\partial x}\left(\int_{S_1}^{z}\left(\frac{1}{\mu}\int_{S_1}^{z'}\frac{\partial \mu}{\partial x}\,dz''\right)dz'\right),$$
$$J_x = \varepsilon^2 \cdot \mu\,\frac{\partial}{\partial x}\,(z - S_1)\,,$$
$$Q_{xx} = \varepsilon^2 \cdot \mu\,\frac{\partial}{\partial x}\left(\int_{S_1}^{z}\left(\frac{1}{\mu}\int_{S_1}^{z'}\frac{\partial}{\partial x}\left(\int_{S_1}^{z''}\rho\,dz'''\right)dz''\right)dz'\right).$$

The series of indices indicated for each coefficient in (17) refers to the series of differentiation operators in the definition of the coefficient. The remaining coefficients in eqs (15) and (16) can be obtained by skipping the differentiation operator corresponding to the position of the 'star' index, e.g.

$$G_{*x} = \varepsilon^2 \mu \cdot \int_{S_1}^{z}\left(\frac{1}{\mu}\int_{S_1}^{z'}\frac{\partial \mu}{\partial x}\,dz''\right)dz'\,. \tag{18}$$

Here we apply this model to layers with constant viscosities; the averaged coefficients referring to viscosity derivatives ($\overline{G_{xx}}$, $\overline{G_{*x}}$, $\overline{z_c G_{xx}}$, $\overline{z_c G_{*x}}$) can therefore be dropped. The horizontal velocity profile is described by

$$v_x(x,z)=V_x+\varepsilon^2 R_x\cdot\int_{S_1}^{z}\frac{dz'}{\mu}+\varepsilon^4\int_{S_1}^{z}\left(\frac{\partial}{\partial x}\int_{S_1}^{z'}\frac{\partial}{\partial x}\left(\int_{S_1}^{z''}\frac{R_x}{\mu}\,dz'''\right)dz''\right)dz'-\varepsilon^2\frac{\partial R_z}{\partial x}\cdot\int_{S_1}^{z}\frac{(z'-S_1)}{\mu}\,dz'$$
$$-\varepsilon^2\int_{S_1}^{z}\left(\frac{1}{\mu}\int_{S_1}^{z'}\frac{\partial}{\partial x}\left(\int_{S_1}^{z''}\rho dz'''\right)dz''\right)dz'+\varepsilon^2\int_{S_1}^{z}\left[\frac{\partial}{\partial x}\int_{S_1}^{z'}\frac{\partial V_x}{\partial x}\,dz''-\frac{4}{\mu}\int_{S_1}^{z'}\frac{\partial}{\partial x}\left(\mu\frac{\partial V_x}{\partial x}\right)dz''\right]dz'-\varepsilon^2\frac{\partial V_z}{\partial x}(z-S_1)\,, \tag{19}$$

where V_x and V_z represent the set of key kinematic functions

$$V_x(x)=v_i(x,z)|_{S_1}\,,$$
$$V_z(x)=v_z(x,z)|_{S_1}\,. \tag{20}$$

A set of kinematic equations describing the motions of the boundaries is necessary to complete the system. These equations are based on the condition of impenetrability and integrated mass balance. For any material boundaries S_m and S_l,

$$\frac{\partial S_m}{\partial t}+v_x|_{S_m}\frac{\partial S_m}{\partial x}=v_z|_{S_m}\,, \tag{21}$$

$$\frac{\partial(S_m-S_l)}{\partial t}+\frac{\partial}{\partial x}\left(\int_{S_l}^{S_m}v_x dz\right)=0\,, \tag{22}$$

$$\int_{S_l}^{S_m}\frac{\partial v_x}{\partial x}\,dz+v_z|_{S_m}^{S_l}=0\,. \tag{23}$$

The last equation represents the integrated incompressibility condition and can be applied to non-material interfaces.

The system of equations (11)–(16) can be simplified for applications to cases with subhorizontally layered lithosphere by analogy with the similar simplification in MP99. This case ('well-stratified lithosphere') is characterized by lateral gradients of density, viscosity and basement S_1 that are so low that they can be neglected, and only those coefficients which have 'stars' as indices are significant. If the reference level, w, is specified as flat, then its horizontal gradients will fall out of the equations

$$4\frac{\partial}{\partial x}\left[\overline{\mu}\frac{\partial V_x}{\partial x}-(4\overline{G_{**}}-\overline{F_{**}})\frac{\partial^3 V_x}{\partial x^3}-\overline{J_*}\frac{\partial^2 V_z}{\partial x^2}+\overline{D_*}\frac{\partial R_x}{\partial x}-\overline{\tilde{D}_{***}}\frac{\partial^3 R_x}{\partial x^3}-\overline{E_*}\frac{\partial^2 R_z}{\partial x^2}+\frac{1}{4}(R_z H+\overline{\overline{p}})\right]+\overline{T_x}=0\,, \tag{24}$$

$$4\frac{\partial^2}{\partial x^2}\left[\overline{z_c\cdot\mu}\frac{\partial V_x}{\partial x}-(4\overline{z_c\cdot G_{**}}-\overline{z_c\cdot F_{**}})\frac{\partial^3 V_x}{\partial x^3}-\overline{z_c\cdot J_*}\frac{\partial^2 V_z}{\partial x^2}+\overline{z_c\cdot D*}\frac{\partial R_x}{\partial x}-\overline{z_c\cdot\tilde{D}_{***}}\frac{\partial^3 R_x}{\partial x^3}-\overline{z_c\cdot E_*}\frac{\partial^2 R_z}{\partial x^2}+\frac{1}{4}(\overline{M_\rho}+R_z\overline{z_c})\right]$$
$$+\frac{\partial}{\partial x}(\overline{z_c T_x})+\overline{\Delta T_z}=0\,. \tag{25}$$

3 TECHNIQUE APPLIED

The behaviour of the ETSA solutions for different boundary conditions is investigated using linear analysis. A set of Maple programs was developed to support these investigations. Maple programs are based on the initial assumptions of MP99 (eqs 19–21 and 34–41) and follow the logic of asymptotic treatment presented in MP99. This significantly decreases the possibility of making mistakes in these long unwieldy equations. It is also possible to investigate variations with additional assumptions, complications or simplifications. Maple and Matlab codes for linear analysis of the full equations were based on Ramberg (1981).

Small sinusoidal perturbations of mean flow are investigated by linear analysis. To investigate the time dependence of the deformation, the system of eqs (11)–(16) was completed by kinematic equations in the form of eqs (21)–(23) and the positions of the boundaries were treated as unknown functions of horizontal coordinates. The unknown functions are given by

$$KF=KF_0+\Delta_{KF}\cdot\mathrm{Trig}\left(\frac{2\pi x}{\lambda}\right)\mathrm{e}^{\alpha t}\,, \tag{26}$$

where KF_0 is the unperturbed solution for unknown functions. The amplitude of the perturbation is $\Delta_{KF}\ll 1$. $\mathrm{Trig}(2\pi x/\lambda)$ represents the sinusoidal distribution of perturbations along the horizontal axis [cosine for X-related key functions (T_x, V_x) and sine for the remaining functions] and parameter α represents the growth rate of perturbations with time. Substituting boundary conditions and the perturbed unknown functions in the form of eq. (26) into the force balance and kinematic equations, neglecting terms with order more than 1 for the amplitudes of the perturbation, and subtracting factorized trigonometric and exponential functions gives a system of equations in the form

$$\boldsymbol{\Delta}_{KF}\cdot\mathbf{A}=0\,, \tag{27}$$

where

$$\mathbf{\Delta}_{KF} = \begin{pmatrix} \Delta_x \\ \Delta_z \\ \Delta_1 \\ \Delta_2 \end{pmatrix}, \qquad \mathbf{A} = \begin{pmatrix} a_{11} & a_{12} & a_{13} & a_{14} \\ a_{21} & a_{22} & a_{23} & a_{24} \\ a_{31} & a_{32} & a_{33}+\alpha & a_{34} \\ a_{41} & a_{42} & a_{43} & a_{44}+\alpha \end{pmatrix}. \tag{28}$$

Here, Δ_x and Δ_z are the amplitudes of perturbations of X- and Z-oriented dynamic key functions and Δ_1 and Δ_2 are perturbations of moving boundaries. Components a_{ij} of the matrix $\mathbf{A}$ are defined by the force balance and the kinematic equations and depend on the wavelength, λ. Eq. (27) refers to the system with two moving boundaries. The last row and column in matrix $\mathbf{A}$ should be dropped to investigate the system with a single moving boundary. Non-trivial solutions of eq. (27) can be obtained only if

$$\det(\mathbf{A}) = 0, \tag{29}$$

and this is the equation that defines the growth rate, α. For cases with two moving boundaries, eq. (29) represents an algebraic quadratic equation with solution

$$\alpha_{1,2} = (-B \pm \sqrt{B^2 - 4A_{\mathrm{dyn}} \det(\tilde{\mathbf{A}})})/2A_{\mathrm{dyn}}, \tag{30}$$

where $\tilde{\mathbf{A}}$ is the matrix of elements $(a_{i,j})$ (i.e. matrix $\mathbf{A}$ but with αs subtracted) and $B = |\tilde{A}_{33}| + |\tilde{A}_{44}|$ is the sum of cofactors to elements a_{33} and a_{44} in matrix $\tilde{\mathbf{A}}$. $A_{\mathrm{dyn}} = (a_{11}a_{22} - a_{12}a_{21})$ represents the dynamic determinant which relates to perturbations of the key functions only in equations for the balance of forces.

The general solution for the evolution of the boundaries is

$$\begin{pmatrix} \Delta_1 \\ \Delta_2 \end{pmatrix} = \begin{pmatrix} g_{11} & g_{12} \\ g_{21} & g_{22} \end{pmatrix} \cdot \begin{pmatrix} \exp(\alpha_1 t) \\ \exp(\alpha_2 t) \end{pmatrix}, \tag{31}$$

where g_{ml} is the projection of the initial perturbation on the external or rheological boundary m with an eigenvector corresponding to eigenvalue α_l. It is not necessary to determine coefficients g_{ij} (Ramberg 1968a) or both eigenvalues in order to investigate the behaviour of the perturbations. This is because of the exponential time dependence in eq. (26): only the larger (principal) of the two eigenvalues determines whether the initial amplitudes of particular wavelengths grow or flatten with time. The results presented below therefore only follow the behaviour of the principal eigenvalue.

Complicated perturbations can be described as a spectrum of sinusoidal perturbations, and the wavelength with the fastest growth rate (eigenvalue) will eventually dominate. The dominant wavelength resulting from most geological processes is more easily recognizable than the kinematic or dynamic characteristics of the process. Therefore, the results presented here are recognized as correct if a defined dominant wavelength compares well with the exact solution.

The dynamic determinant introduced in eq. (30) plays a significant role in the behaviour of asymptotic systems. In the full system of equations, the constant sign of this determinant ($\neq 0$) demonstrates the ellipticity of the original equation system. However, the level of approximation we apply for this determinant can change in sign. The ranges of parameters which result in a constant sign for the dynamic determinant determine whether the model can be used. The change in sign of A_{dyn} results in singularity of the solution (30). The proper use of partitioning coefficient a_z can increase the range of ellipticity of the governing system of the ETSA. We will not discuss the details of the behaviour of this determinant in every example; instead we will present the results of the most appropriate choice for a_z and try to explore the simple rules empirically to match the correct solutions.

The reference surface w involved in evaluations of moments (eqs 12 and 16) is a free parameter of the ETSA (MP99) which cannot change the results but is able to simplify the treatment. Linear analyses presented below do not depend on this parameter since w falls out of the linearized system eq. (29). However, we emphasize the significance of the reference surface by describing possible choices in each example.

4 EXAMPLE A: EVOLUTION OF A LAYER DRIVEN BY BASAL VELOCITY (SS CASE)

Consider a single lithospheric layer with constant density and viscosity. The lower surface $S_1(x)$ is subjected to a prescribed velocity field ($V_0 = \{V_{0,x}(x), V_{0,z}(x)\}$), while the upper surface $S_2(x)$ is stress-free:

$$\begin{aligned} &V_x = V_{0,x}, \qquad V_z = V_{0,z}, \\ &T_x|_{S_2} = 0, \qquad T_z|_{S_2} = 0; \end{aligned} \tag{32}$$

therefore,

$$\overline{T_x} = T_x|_{S_1}\,, \qquad \overline{T_z} = T_z|_{S_1}\,. \tag{33}$$

Since both the kinematic and the dynamic boundary conditions are set on horizontal boundaries, the key unknown functions have to include two dynamic functions (MP99):

$$R_x(x)\,, \quad \tilde{R}_z(x)\,, \quad S_1(x)\,, \quad S_2(x)\,, \tag{34}$$

where $\tilde{R}_z = (\overline{\rho} - \overline{T_z})$. The horizontal projection of boundary force balance in eqs (13) gives

$$\overline{T_x} = -R_x^{(1)} + \left(4\mu\,\frac{\partial V_{0,x}}{\partial x} + R_z\right)\frac{\partial S_1}{\partial x}\,. \tag{35}$$

The vertical partitioning is defined by eqs (14):

$$R_z = a_z\tilde{R}_z - \overline{\rho}\,, \qquad \overline{T_z^{(1)}} = \varepsilon^{-2}\tilde{R}_z\,. \tag{36}$$

Substitution of boundary conditions and partitioning into eqs (11)–(12) gives

$$-R_x + 2\,\frac{\partial\overline{\tau_{xx}}}{\partial x} + a_z\left(H\,\frac{\partial\tilde{R}_z}{\partial x} + \tilde{R}_z\,\frac{\partial S_2}{\partial x}\right) - \rho H\,\frac{\partial S_2}{\partial x} + 4\mu\,\frac{\partial S_1}{\partial x}\cdot\frac{\partial V_{0,x}}{\partial x} = 0\,, \tag{37}$$

$$\begin{aligned}&\frac{\partial^2}{\partial x^2}\left[2\overline{z_c\tau_{xx}} - \rho\left(\overline{z_c}^{(1)} - \frac{H^3}{6}\right) + a_z\tilde{R}_z\overline{z_c}^{(2)}\right] + \frac{\partial}{\partial x}\left[\left(2\overline{\tau_{xx}} - \rho\,\frac{H^2}{2} + a_z\tilde{R}_z\right)\frac{\partial w}{\partial x}\right]\\ &\quad + \frac{\partial}{\partial x}\left[h_w\left(R_x^{(1)} - \left(4\mu\,\frac{\partial V_{0,x}}{\partial x} + a_z\tilde{R}_z - \overline{\rho}\right)\frac{\partial S_1}{\partial x}\right)\right] - \frac{1}{\varepsilon^2}\,\tilde{R}_z = 0\,.\end{aligned} \tag{38}$$

After substitution of coefficients evaluated for this case into eq. (15), the horizontal viscous stress is

$$\begin{aligned}\overline{\tau_{xx}}(x) = {}& 2\mu H\,\frac{\partial V_{0,x}}{\partial x} + \varepsilon^2 H\left(H\,\frac{\partial R_x}{\partial x} - 2\,\frac{\partial S_1}{\partial x}\,R_x\right) - \varepsilon^4 H^3\left(\frac{H}{12}\,\frac{\partial^3 R_x}{\partial x^3} - \frac{\partial S_1}{\partial x}\,\frac{\partial^2 R_x}{\partial x^2}\right) + a_z\varepsilon^2\left(H^2\,\frac{\partial S_1}{\partial x}\,\frac{\partial\tilde{R}_z}{\partial x} - \frac{H^3}{3}\,\frac{\partial^2\tilde{R}_z}{\partial x^2}\right)\\ &+ \varepsilon^2\rho\left(\frac{H^3}{3}\,\frac{\partial^2 S_2}{\partial x^2} - H^2\,\frac{\partial S_1}{\partial x}\cdot\frac{\partial S_2}{\partial x}\right) + \varepsilon^2\mu\left(2H\left(\frac{\partial S_1}{\partial x}\right)^2 - H^2\,\frac{\partial^2 S_1}{\partial x^2}\right)\frac{\partial V_{0,x}}{\partial x} + \varepsilon^2\left(H^2\,\frac{\partial^2 V_{0,z}}{\partial x^2} - 2H\,\frac{\partial S_1}{\partial x}\,\frac{\partial V_{0,z}}{\partial x}\right)\\ &+ 2\varepsilon^2\mu H^2\,\frac{\partial S_1}{\partial x}\cdot\frac{\partial^2 V_{0x}}{\partial x^2} - \varepsilon^2\mu H^3\,\frac{\partial^3 V_{0x}}{\partial x^3}\,.\end{aligned} \tag{39}$$

The coefficients $\tilde{D}_{xxx}$ and $\tilde{D}_{*xx}$ were dropped as they are smaller than $\tilde{D}_x$ and $\tilde{D}_*$ by a factor ε^2 and refer to the same unknown functions. Terms $z_c\tilde{D}_{xxx}$ and $z_c\tilde{D}_{*xx}$ were dropped for the same reason in the following expression for the averaged moment of horizontal viscous stress (from eq. 16):

$$\begin{aligned}\overline{z_c\tau_{xx}}(x) = {}& 2\mu\overline{z_c}\,\frac{\partial V_{0,x}}{\partial x} + 2\varepsilon^2\left(\overline{z_c}^{(1)}\,\frac{\partial R_x}{\partial x} - \overline{z_c}\,\frac{\partial S_1}{\partial x}\,R_x\right) - 2\varepsilon^4\left(\overline{z_c}^{(3)}\,\frac{\partial^3 R_x}{\partial x^3} - \overline{z_c}^{(2)}\,\frac{\partial S_1}{\partial x}\,\frac{\partial^2 R_x}{\partial x^2}\right) + 2a_z\varepsilon^2\left(\overline{z_c}^{(1)}\,\frac{\partial S_1}{\partial x}\,\frac{\partial\tilde{R}_z}{\partial x} - \overline{z_c}^{(2)}\,\frac{\partial^2\tilde{R}_z}{\partial x^2}\right)\\ &+ 2\varepsilon^2\rho\left(\overline{z_c}^{(2)}\,\frac{\partial^2 S_2}{\partial x^2} - \overline{z_c}^{(1)}\,\frac{\partial S_1}{\partial x}\cdot\frac{\partial S_2}{\partial x}\right) + 2\varepsilon^2\mu\left(\overline{z_c}\left(\frac{\partial S_1}{\partial x}\right)^2 - \overline{z_c}^{(1)}\,\frac{\partial^2 S_1}{\partial x^2}\right)\frac{\partial V_{0,x}}{\partial x} + 2\varepsilon^2\left(\overline{z_c}^{(1)}\,\frac{\partial^2 V_{0,z}}{\partial x^2} - \overline{z_c}\,\frac{\partial S_1}{\partial x}\,\frac{\partial V_{0,z}}{\partial x}\right)\\ &+ 4\varepsilon^2\mu\overline{z_c}^{(1)}\,\frac{\partial S_1}{\partial x}\cdot\frac{\partial^2 V_{0x}}{\partial x^2} - 6\varepsilon^2\mu\overline{z_c}^{(2)}\,\frac{\partial^3 V_{0x}}{\partial x^3}\,.\end{aligned} \tag{40}$$

Two kinematic equations should be added to complete the system:

$$\frac{\partial S_1}{\partial t} + V_{0,x}\,\frac{\partial S_1}{\partial x} = V_{0,z}\,, \tag{41}$$

$$\frac{\partial H}{\partial t} + \frac{\partial}{\partial x}\,(V_{0,x}H) + \varepsilon^2\,\frac{\partial}{\partial x}\left[\frac{H^2}{2}\left(\frac{R_x}{\mu} - \frac{\partial S_1}{\partial x}\cdot\frac{\partial V_{0,x}}{\partial x} - \frac{\partial V_{0,z}}{\partial x}\right)\right] + \varepsilon^2\,\frac{\partial}{\partial x}\left[\frac{H^3}{6}\left(\frac{\rho}{\mu}\cdot\frac{\partial S_2}{\partial x} - \frac{1}{\mu}\cdot\frac{\partial R_z}{\partial x} - \frac{1}{2}\,\frac{\partial^2 V_{0,x}}{\partial x^2}\right)\right] = 0\,. \tag{42}$$

Eq. (42) is developed by integrating the velocity field over the depth and substituting the result into eq. (22). The velocity field is

$$v_x(x, z) = V_{0,x} + \varepsilon^2(z - S_1)\left(\frac{R_x}{\mu} - \frac{\partial V_{0,x}}{\partial x}\cdot\frac{\partial S_1}{\partial x} - \frac{\partial V_{0,z}}{\partial x}\right) + \varepsilon^2\,\frac{(z - S_1)^2}{2}\left(\frac{\rho}{\mu}\cdot\frac{\partial S_2}{\partial x} - 3\,\frac{\partial^2 V_{0,x}}{\partial x^2} - \frac{1}{\mu}\,\frac{\partial\tilde{R}_z}{\partial x}\right). \tag{43}$$

4.1 Simple cases

4.1.1 The SS$^+$ approach

Subtracting ε terms in force balance eqs (37)–(39) allows a simplified solution for the key dynamic functions:

$$\begin{aligned} &\tilde{R}_z = 0\,, \\ &R_x = 4\mu \frac{\partial}{\partial x}\left(H \frac{\partial V_{0,x}}{\partial x}\right) + 4\mu \frac{\partial V_{0,x}}{\partial x} \cdot \frac{\partial S_1}{\partial x} - \rho H \cdot \frac{\partial S_2}{\partial x}\,. \end{aligned} \tag{44}$$

Substitution of the solution of eq. (44) into the expression for the velocity field eq. (43) yields

$$\begin{aligned} v_x(x, z) = V_{0,x} - \varepsilon^2 \frac{\rho}{\mu}\left(H - \frac{z - S_1}{2}\right)(z - S_1) \cdot \frac{\partial S_2}{\partial x} + \varepsilon^2 (z - S_1) \frac{\partial V_{0,x}}{\partial x} \cdot \frac{\partial (4S_2 - S_1)}{\partial x} \\ + \varepsilon^2 \left(4H(z - S_1) - \frac{3}{2}(z - S_1)^2\right) \frac{\partial^2 V_{0,x}}{\partial x^2} - \varepsilon^2 (z - S_1) \frac{\partial V_{0,z}}{\partial x}\,. \end{aligned} \tag{45}$$

Evolution of the layer can be described by

$$\frac{\partial H}{\partial t} + \frac{\partial}{\partial x}(V_{0,x} H) - \varepsilon^2 \frac{\partial}{\partial x}\left[H^3 \left(\frac{\rho}{3\mu} \cdot \frac{\partial S_2}{\partial x} - \frac{3}{2} \frac{\partial^2 V_{0,x}}{\partial x^2}\right)\right] + \varepsilon^2 \frac{\partial}{\partial x}\left[\frac{H^2}{2}\left(\frac{\partial (4S_2 - S_1)}{\partial x} \cdot \frac{\partial V_{0,x}}{\partial x} - \frac{\partial V_{0,z}}{\partial x}\right)\right] = 0\,. \tag{46}$$

This approach was derived by the authors (1995, unpublished) and applied to modelling of the evolution of salt extrusions (Talbot *et al.* 1998). The SS$^+$ approach can handle a larger range of basal velocities than the pure SS approach (described below).

4.1.2 The SS approach

Results with accuracy up to $O(\varepsilon^4)$ can be obtained for 'slow' basal velocities ($V_{SS} \sim \varepsilon^2 V_0$) by neglecting terms containing both basal velocity and ε^2 and rescaling ($t' = t/\varepsilon^2$, $v' = \varepsilon^2 v$):

$$\begin{aligned} &v'_x(x, z) = V_{SS,x} - \frac{\rho}{2\mu} \cdot \frac{\partial S_2}{\partial x} \cdot (z - S_1)(2S_2 - S_1 - z)\,, \\ &\frac{\partial H}{\partial t'} + \frac{\partial}{\partial x}(V_{SS,x} H) - \frac{\rho}{\mu} \frac{\partial}{\partial x}\left(\frac{H^3}{3} \frac{\partial S_2}{\partial x}\right) = 0\,. \end{aligned} \tag{47}$$

Eqs (47) represent the SS approach (Lobkovsky & Kerchman 1991; Medvedev 1993; Buck & Sokoutis 1994). Comparison of eqs (47) with the more accurate expressions, eqs (43) and (42), emphasizes the need to scale the basal velocity correctly (Lobkovsky & Kerchman 1991) and use a full description for deformation subjected to singular boundary conditions (Buck & Sokoutis 1994; Royden 1996).

4.2 Isostatic adjustment

Consider the development of small perturbations in the top of an initially horizontal layer without lateral forces and with basal velocities ($V_{0,x} = 0$, $V_{0,z} = 0$). This simple test illustrates the isostatic adjustment of perturbations in a single lithospheric layer. Previous thin-sheet approximations demonstrated increasing adjustment rates with decreasing wavelengths; this does not compare well with natural examples, which demonstrate the existence of dominant wavelengths. Ramberg (1968b) demonstrated this phenomenon analytically.

The solution of the equations gives the unperturbed flow parameters

$$R_x = 0\,, \qquad \tilde{R}_z = 0\,, \qquad H = H_0\,. \tag{48}$$

Small periodic perturbations have the form of eq. (26):

$$\delta H = \delta S_2 = \mathrm{e}^{\alpha t} \Delta_2 \sin(\omega x)\,, \quad \delta R_x = \mathrm{e}^{\alpha t} \Delta_x \cos(\omega x)\,, \quad \delta \tilde{R}_z = \mathrm{e}^{\alpha t} \Delta_z \sin(\omega x)\,. \tag{49}$$

Note that no perturbations were considered along the bottom boundary as the motion of boundary S_1 is defined exactly by the boundary conditions (eq. 41). Substitution of the perturbed fields and a zero basal velocity into eqs (37)–(40) gives the general solution in the form of eq. (30).

The dependence of the growth factor, α, on the wavelength of the perturbations, λ, for this simple case of isostatic adjustment calculated using the ETSA and the exact solution (after Ramberg 1968a,b) shows not only qualitative similarity but also good quantitative reproducibility (Fig. 3). The ETSA results have a low partitioning dependence if $a_z \in [0, 1]$. Application of the SS approach (eq. 47) demonstrates the common behaviour of low-order thin-sheet approximations: shorter waves develop faster.

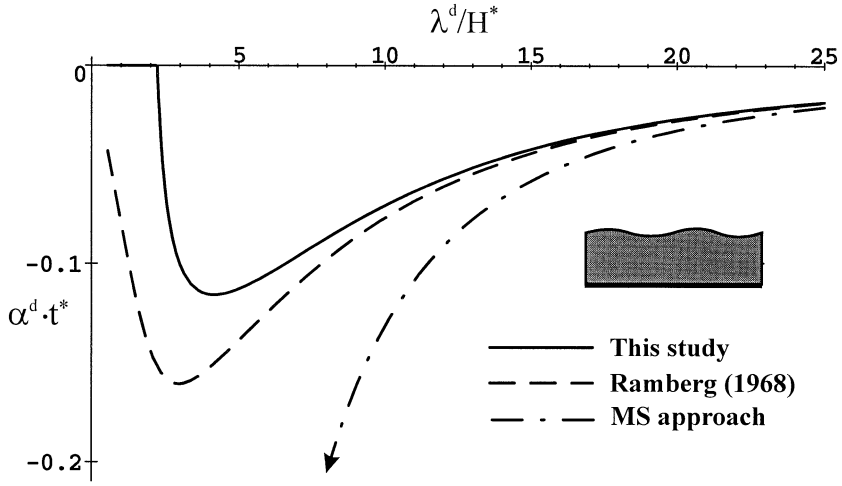

Figure 3. Example A. Spectrum illustrating the dependence of dimensionless growth rate on wavelength for isostatic adjustment of an upper boundary perturbation in a single-layer system ($a_z=0$).

5 EXAMPLE B: EVOLUTION OF A TWO-LAYER SYSTEM DRIVEN BY BASAL VELOCITY

Our second example is a system with two layers (e.g. crustal and subcrustal lithosphere) with constant densities (ρ_1 and ρ_2 for bottom and top layers respectively) and viscosities (μ_1 and μ_2) and differs from the first example only in rheology. $S_*(x)$ is the rheological boundary between the two layers. Note that the viscosity difference may be significant. The boundary conditions, key functions and partitioning are the same as in example A (eqs 32–36) with only μ changed to μ_1 on the bottom boundary (eq. 35). The boundary and rheological settings result in the 2-D system of force balance (from eqs 11–12)

$$-R_x+2\frac{\partial\overline{\tau_{xx}}}{\partial x}+a_z\left(H\frac{\partial\tilde{R}_z}{\partial x}+\tilde{R}_z\frac{\partial S_2}{\partial x}\right)-\rho_2 H\frac{\partial S_2}{\partial x}+\Delta_\rho h_1\frac{\partial S_*}{\partial x}+4\mu_1\frac{\partial S_1}{\partial x}\cdot\frac{\partial V_{0,x}}{\partial x}=0\,, \tag{50}$$

$$\frac{\partial^2}{\partial x^2}\left[2\overline{z_c\tau_{xx}}+\overline{M_\rho}+(a_z\tilde{R}_z-\overline{\rho})\overline{z_c}\right]+\frac{\partial}{\partial x}\left[(2\overline{\tau_{xx}}+(a_z\tilde{R}_z-\overline{\rho})H+\overline{\overline{\rho}})\frac{\partial w}{\partial x}\right]$$
$$+\frac{\partial}{\partial x}\left[h_w\left(R_x^{(1)}-\left(4\mu_1\frac{\partial V_{0,x}}{\partial x}+a_z\tilde{R}_z-\overline{\rho}\right)\frac{\partial S_1}{\partial x}\right)\right]-\frac{1}{\varepsilon^2}\tilde{R}_z=0\,. \tag{51}$$

The averaged horizontal viscous stress and averaged moment of the horizontal viscous stress have the same form as for the general 2-D case in eqs (15) and (16). The evaluation of the coefficients is carried out in Appendix A. The viscosity contrast between the two layers results in the appearance of a viscosity heterogeneity coefficient δ_μ and its momentum M_μ in the equations. If $\mu_1\ll\mu_2$, these two coefficients introduce singularities into the equations since $\delta_\mu, M_\mu\gg1$. In this case the coefficients presented in Appendix A can be simplified by dropping insignificant terms.

The position of the reference surface $w(x)$ is significant in this case. For example, putting the reference surface $w=(S_2+S_3)/2$ reduces the singular terms (which involve the viscosity ratio) in vertical force balance, because then the momentum of viscosity heterogeneity $M_\mu=0$. This is convenient for numerical calculations and balances analytical solutions. However, the simplest presentation of the averaged moment of horizontal stress is obtained by putting $w=S_1$ (see Appendix A).

The horizontal projection of the velocity field for $z<S_*$ is

$$v_x(x,z)=V_{0,x}+\varepsilon^2(z-S_1)\left(\frac{R_x}{\mu_1}-\frac{\partial V_{0,x}}{\partial x}\cdot\frac{\partial S_1}{\partial x}-\frac{\partial V_{0,z}}{\partial x}\right)-\frac{3}{2}\varepsilon^2(z-S_1)^2\cdot\frac{\partial^2 V_x}{\partial x^2}+\varepsilon^2\frac{(z-S_1)^2}{2\mu_1}K_z\,, \tag{52}$$

where

$$K_z=\left(\rho_2\frac{\partial S_2}{\partial x}-\Delta_\rho\frac{\partial S_*}{\partial x}-a_z\frac{\partial\tilde{R}_z}{\partial x}\right)$$

and the horizontal projection of the velocity for $z>S_*$ is

$$v_x(x,z)=V_{0,x}+\varepsilon^2\left(\frac{h_1}{\mu_1}+\frac{(z-S_*)}{\mu_2}\right)R_x-\varepsilon^2(z-S_1)\left(\frac{\partial V_{0,x}}{\partial x}\cdot\frac{\partial S_1}{\partial x}+\frac{\partial V_{0,z}}{\partial x}\right)$$
$$-\varepsilon^2\left[\frac{3}{2}(z-S_1)^2+4h_1\frac{\Delta_\mu}{\mu_2}(z-S_*)\right]\frac{\partial^2 V_{0,x}}{\partial x^2}+\varepsilon^2\left(\frac{h_1^2}{2\mu_1}+\frac{h_1(z-S_*)}{\mu_2}+\frac{(z-S_*)^2}{2\mu_2}\right)K_z+\Delta_\rho\frac{(z-S_*)^2}{2\mu_2}\frac{\partial S_*}{\partial x}\,. \tag{53}$$

Evolution of the layers can be described by eqs (22) after integrating the velocity field

$$\frac{\partial h_1}{\partial t}+\frac{\partial}{\partial x}\left(V_{0,x}h_1\right)+\frac{\varepsilon^2}{2}\frac{\partial}{\partial x}\left[h_1^2\left(\frac{R_x}{\mu_1}-\frac{\partial V_{0,x}}{\partial x}\cdot\frac{\partial S_1}{\partial x}-\frac{\partial V_{0,z}}{\partial x}\right)-h_1^3\frac{\partial^2 V_{0,x}}{\partial x^2}+\frac{h_1^3 K_z}{3\mu_1}\right]=0\,, \tag{54}$$

$$\begin{aligned}&\frac{\partial H}{\partial t}+\frac{\partial}{\partial x}\left(V_{0,x}H\right)+\varepsilon^2\frac{\partial}{\partial x}\left[\left(\frac{h_1 H}{\mu_1}+\frac{h_2^2}{2\mu_2}\right)R_x-\frac{H^2}{2}\left(\frac{\partial V_{0,z}}{\partial x}+\frac{\partial V_{0,x}}{\partial x}\cdot\frac{\partial S_1}{\partial x}\right)\right.\\&\left.-\left(\frac{H^3}{2}-2h_2^2h_1\frac{\Delta_\mu}{\mu_2}\right)\frac{\partial^2 V_{0,x}}{\partial x^2}+\left(\frac{h_1^3}{6\mu_1}+\frac{h_1^2h_2}{2\mu_1}+\frac{h_1h_2^2}{2\mu_2}+\frac{h_2^3}{6\mu_2}\right)K_z+\Delta_\rho\frac{h_2^3}{6\mu_2}\cdot\frac{\partial S_*}{\partial x}\right]=0\,.\end{aligned} \tag{55}$$

5.1 Simple cases

5.1.1 The SS approach

Zanemonetz *et al.* (1976) and Medvedev (1993) investigated this model under the condition of 'slow' basal velocity $V_{SS}\sim\varepsilon^2 V_0$. The governing equations of this approach can be obtained by neglecting terms containing both basal velocity and ε^2 in eqs (50)–(55) and rescaling ($t'=t/\varepsilon^2$, $v'=\varepsilon^2 v$):

$$\tilde{R}_z^{(ms)}=0\,,\quad R_x^{(ms)}(x)=-\rho_2 H\frac{\partial S_2}{\partial x}+\Delta_\rho h_1\frac{\partial S_*}{\partial x}\,. \tag{56}$$

The velocity field for $z<S_*$ is

$$v_x'(x,z)=V_{SS,x}+\frac{(z-S_1)}{2\mu_1}\left(\rho_2(z-S_1-2H)\frac{\partial S_2}{\partial x}-\Delta_\rho(z-S_1-2h_1)\frac{\partial S_*}{\partial x}\right), \tag{57}$$

and for $z>S_*$,

$$v_x'(x,z)=V_{SS,x}+\frac{\rho_2}{2\mu_2}\frac{\partial S_2}{\partial x}\left[(z-S_1)(z-S_1-2H)+h_1h_2\delta_\mu\right]+\varepsilon^2\frac{\Delta_\rho h_1^2}{2\mu_1}\frac{\partial S_*}{\partial x}\,. \tag{58}$$

Evolution of the layers is described by

$$\begin{aligned}&\frac{\partial h_1}{\partial t'}+\frac{\partial}{\partial x}\left[V_{SS,x}h_1+\frac{h_1^2}{6\mu_1}\left(\rho_2(h_1-3H)\frac{\partial S_2}{\partial x}+2\Delta_\rho h_1\frac{\partial S_*}{\partial x}\right)\right]=0\,,\\&\frac{\partial H}{\partial t'}+\frac{\partial}{\partial x}\left[V_{SS,x}H+\frac{\Delta_\rho h_1^2}{\mu_1}\left(\frac{h_1}{3}+\frac{h_2}{2}\right)\frac{\partial S_*}{\partial x}-\rho_2\left(\frac{2h_1^3}{3\mu_1}+\frac{2h_2^3}{3\mu_2}+\frac{h_1h_2H}{\mu_1}\right)\frac{\partial S_2}{\partial x}\right]=0\,.\end{aligned} \tag{59}$$

This approach is applicable only to situations with low viscosity contrasts (Medvedev 1993).

5.1.2 The Ellis et al. *(1995) model*

Ellis *et al.* (1995) investigated a similar case with the additional assumptions of a thinner bottom layer with constant thickness, $h_1=\text{const}\ll h_2$, a more competent upper layer $\mu_2\gg\mu_1$ and $h_1/\mu_1\gg h_2/\mu_2$.

Ellis *et al.* (1995) applied a dynamic vertical boundary condition on the base which is not quite the same as the boundary conditions in eqs (32)–(33). However, the simplicity of balancing the vertical forces suggested by Ellis *et al.* (1995) allows a comparison of the analytical results of this approach with the ETSA in this section by adding Airy isostasy as in eq. (63).

Let us consider the behaviour of eqs (50)–(55) using the assumptions of Ellis *et al.* (1995). The vertical force balance eq. (51) is simplified by neglecting all ε terms to give the lithostatic condition $\tilde{R}_z=0$. Consideration of the velocity field in the upper layer (eq. 53) allows the extraction of two leading terms:

$$v_x(x,z)\approx V_{0,x}+\varepsilon^2\frac{h_1}{\mu_1}R_x=v_x|_{S_*}=\overline{v_x}(x)\quad z>S_*\,. \tag{60}$$

This shows the independence of the horizontal velocity in the upper layer at the level of approximation presented here. Hence,

$$R_x=\frac{\mu_1}{\varepsilon^2 h_1}\left(\overline{v_x}-V_{0,x}\right). \tag{61}$$

Substituting eq. (61) into the horizontal force balance in eqs (50) and (15) gives, after neglecting all ε terms and neglecting insignificant terms due to the condition $\mu_1 \ll \mu_2$ (the latter is indicated by $\approx$),

$$\begin{aligned} 2\frac{\partial \overline{\tau_{xx}}}{\partial x} &= \rho_2 H \frac{\partial S_2}{\partial x} - \Delta_\rho h_1 \frac{\partial S_*}{\partial x} + \frac{\mu_1}{\varepsilon^2 h_1}(\overline{v_x} - V_{0,x}), \\ \overline{\tau_{xx}} &= 2\overline{\mu}\frac{\partial V_{0,x}}{\partial x} + \varepsilon \overline{D_x} R_x + \varepsilon \overline{D_*}\frac{\partial R_x}{\partial x} \approx 2\mu_2 h_2 \frac{\partial \overline{v_x}}{\partial x}. \end{aligned} \tag{62}$$

Application of the Airy scheme of isostasy (Turcotte & Schubert 1982) on the basis of mantle density ρ_m and assuming a constant thickness for the bottom layer gives

$$\rho_2 H \frac{}{\partial S_2}\,\partial x - \Delta_\rho h_1 \frac{\partial S_*}{\partial x} = \rho_2 h_2 \frac{\partial S_2}{\partial x} = \frac{\rho_2(\rho_m - \rho_2)}{2\rho_m}\frac{\partial h_2^2}{\partial x}. \tag{63}$$

Substitution of eq. (63) into eq. (62) gives the equation derived by Ellis *et al.* (1995) and proves the applicability of Couette flow for description of deformations in the bottom layer:

$$\begin{aligned} &\frac{\partial}{\partial x}\left(h_2 \frac{\partial \overline{v_x}}{\partial x}\right) = \frac{\rho_2(\rho_m - \rho_2)}{8\rho_m \mu_2}\frac{\partial h_2^2}{\partial x} + \frac{\mu_1}{4\varepsilon^2 \mu_2 h_1}(\overline{v_x} - V_{0,x}), \\ &v_x(x, z) = V_{0,x} + \frac{(z - S_1)}{h_1}(\overline{v_x} - V_{0,x}), \qquad z < S_*, \\ &v_x(x) = \overline{v_x}, \qquad z > S_*. \end{aligned} \tag{64}$$

We describe this case as a variation of the SS approach because deformation is defined by the horizontal boundary velocities prescribed along the base. In contrast, Ellis *et al.* (1995) recognized their model as an extension of the PS approach (following the model of Wdowinski *et al.* 1989). The model presented by Ellis *et al.* (1995) is not completely supported by the asymptotic analysis described in the ETSA formulation because eq. (61) is not fully compatible with the simple vertical force balance ($\tilde{R}_z = 0$) (*cf*. eq. 51). However, the model of Ellis *et al.* (1995) has a number of advantages for the modelling of rheologically stratified systems.

5.2 Rayleigh–Taylor instability

In additional to the boundary conditions of Example B (eqs 32–33), the basement S_1 in this case is a constant in time and space and $V_0 = 0$. The density contrast $\Delta_\rho = \rho_2 - \rho_1 > 0$ illustrates the gravity instability in this test. The linear analysis is similar to that performed in Example A with an additional equation to describe the motion of the rheological boundary (eq. 54).

Fig. 4 compares the results for different approaches. The SS approach behaves well only for long wavelengths and tends to infinity for short wavelengths (not indicated in Fig. 5 because of the difference in scale).

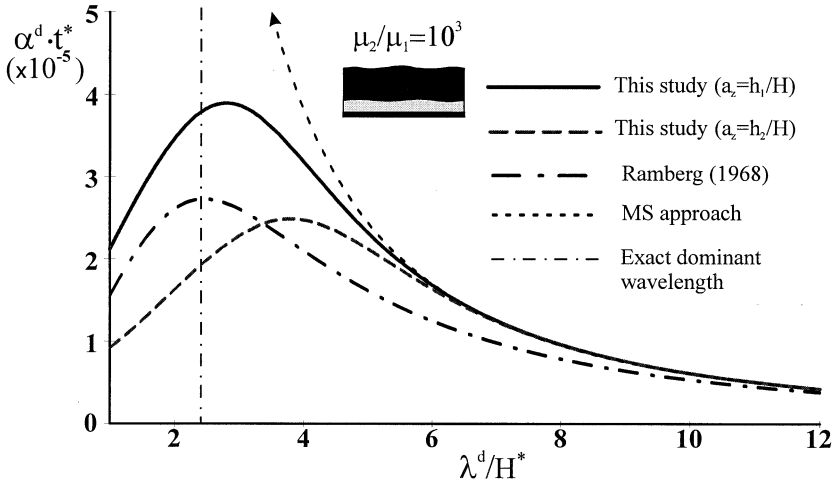

Figure 4. Example B. Comparison of applying the different approaches to the growth of Rayleigh–Taylor instabilities in two-layer systems with free upper surfaces and no-slip bottom boundaries. Comparing the ETSA results for different partitioning coefficients a_z illustrates the criteria of correctness: the proximity to the correct wavelength, not the correct growth rate. The partitioning coefficient $a_z = h_1/H$ performs well over a wide range of geometries and rheological conditions. The SS approach works well for long wavelengths but not for short wavelengths ($h_1/H = 0.1$, $\rho_2 = 1.2 \cdot \rho_1$).

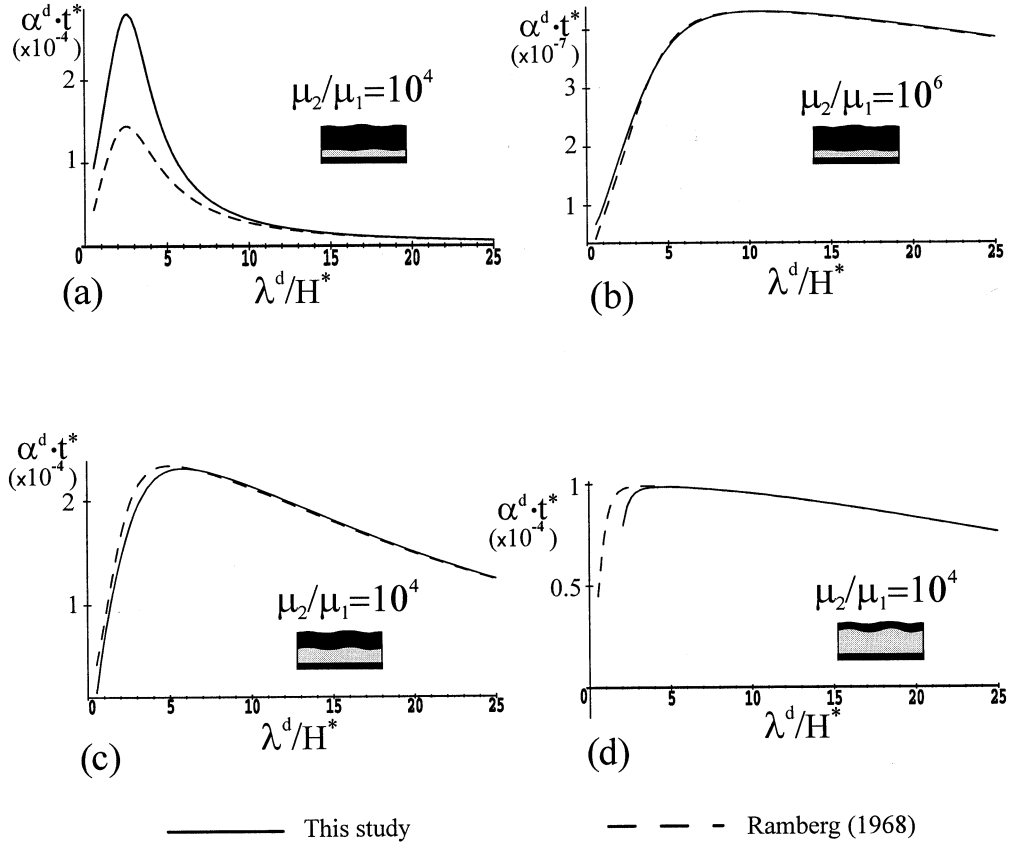

Figure 5. Example B. Comparison of the influence of different factors on the growth rate of Rayleigh–Taylor instabilities in two-layer systems with free upper surfaces and no-slip bottom boundaries. (a) and (b) illustrate the influence of different viscosity contrasts. (a), (c) and (d) show spectra due to differences in geometry: (upper layer thickness/full thickness) = 0.1, 0.5 and 0.8 respectively ($\rho_2 = 2\rho_1$, $a_z = h_1/H$).

Our investigations into the influence of partitioning emphasize the significance of coefficient a_z. ETSA applications with different partitioning coefficients were compared with the exact solution (after Ramberg 1968a). This comparison (Fig. 4) illustrates the criteria we used to define the correct solution. Even the maximum growth rate is about double the exact solution for $a_z = h_1/H$; this result is treated as more accurate than results based on other values of a_z since the dominant wavelength is closer to the exact dominant wavelength. Our experience suggests that the coefficient $a_z = h_1/H$ is appropriate. This means that the most appropriate boundary condition to be satisfied at a low level of approximation (eqs 8 and 36) is that closest to the most intense rheological gradient within the model. This is well demonstrated by Figs 4 and 5. Nevertheless, the results demonstrate the great advantages of ETSA compared to previous thin-sheet approaches, even with the use of inappropriate a_z.

There is good agreement between the ETSA and the exact solution for different rheological settings (Fig. 5). Fig. 6 shows that the dominant wavelength depends on the viscosity contrast. In contrast to general opinion that this exhibits a cubic root law behaviour (e.g. Whitehead 1988), Fig. 6 indicates that the dominant wavelength varies much closer to the sixth-order root of the viscosity contrast, probably because of the influence of the upper stress-free surface.

5.3 Systems driven by basal velocity

This section considers the influence of applying a basal horizontal velocity. The vertical component of the basal velocity is set as $V_{0,z} = 0$ and the bottom boundary is constant in time and space ($S_1 = \text{const}$). The basal horizontal velocity is defined by a constant gradient $V_{0,x} = V^* x$. The unperturbed flow is described by

$$R_x = 0, \quad \tilde{R}_z = 0, \quad v_x = V^* x, \quad v_z = -V^*(z - S_1), \quad H = H_0 \exp(-V^* t). \tag{65}$$

The linear analysis was performed for the case $V^* < 0$, which laterally compresses the system (Figs 7 and 8).

Comparison of Figs 7(a) and (b) shows that the dominant wavelength depends more on the viscosity contrast then on the magnitude of the velocity gradient, as suggested by Ellis *et al.* (1995) (although we cannot compare our results with theirs directly because our boundary conditions differ).

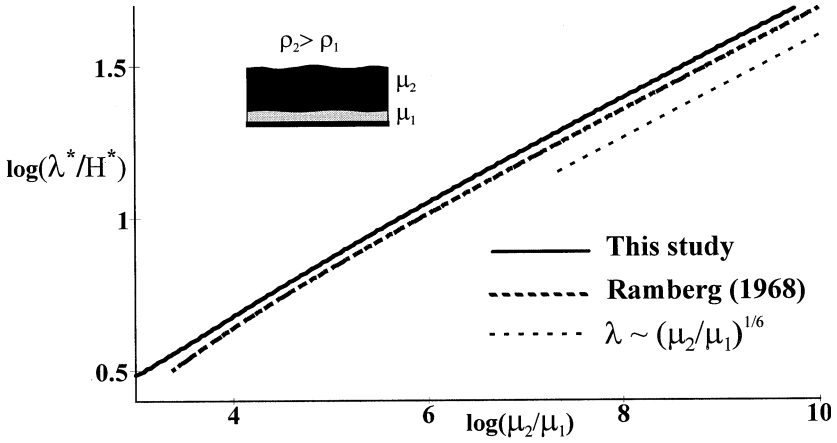

Figure 6. Example B. Dominant wavelength versus viscosity ratio for two-layer systems with free upper surfaces and no-slip bottom boundaries with a density instability. Comparison of results from this study and Ramberg (1968a,b). Line $\lambda \sim \sqrt[6]{\mu_2/\mu_1}$ illustrates the asymptotic behaviour ($\rho_2 = 2\rho_1$, $h_1/H = 0.1$, $a_z = 0.1$).

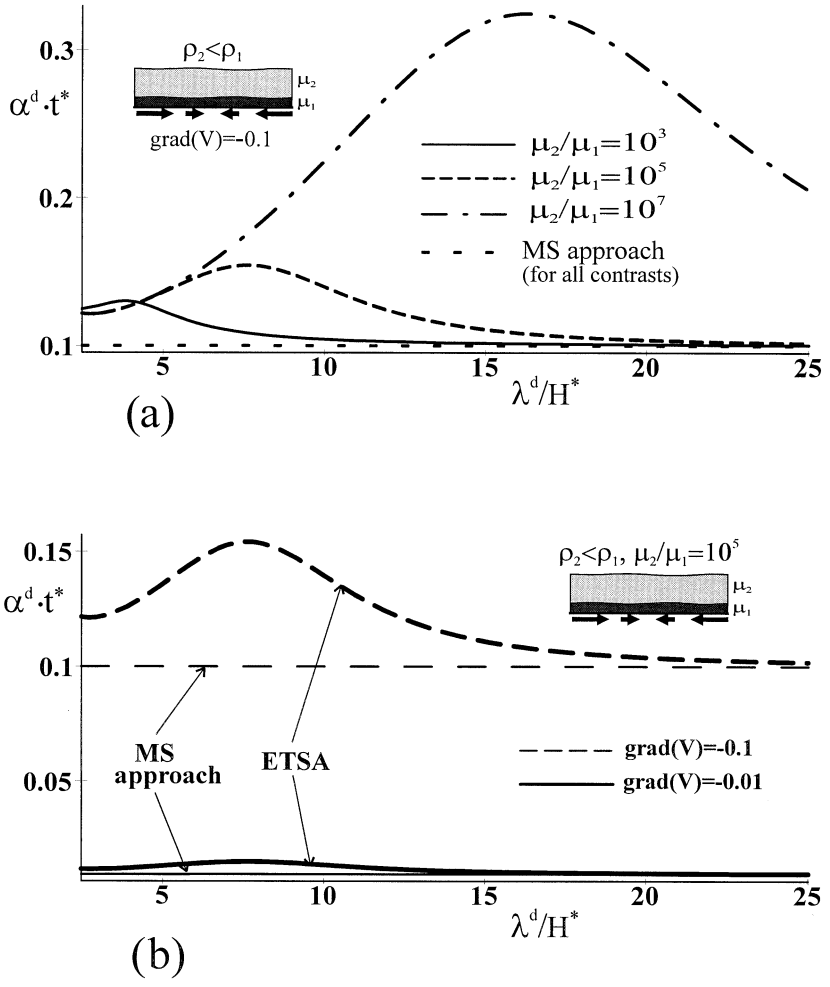

Figure 7. Example B. Basal-driven compression with a constant gradient of velocity along the bottom boundary. (a) Comparison of spectra for different viscosity ratios. (b) Comparison of spectra for different basal velocity gradients demonstrating the low dependence of dominant wavelength on velocity gradient. The SS approach (after Medvedev 1993) shows independence from rheology and is controlled mostly by the velocity gradient. The scaling factor for the dimensionless velocity gradient is $(\rho^* g H^*/\mu^*)$ ($h_1/H = 0.1$, $\rho_2 = 0.8\rho_1$, $a_z = 0.1$).

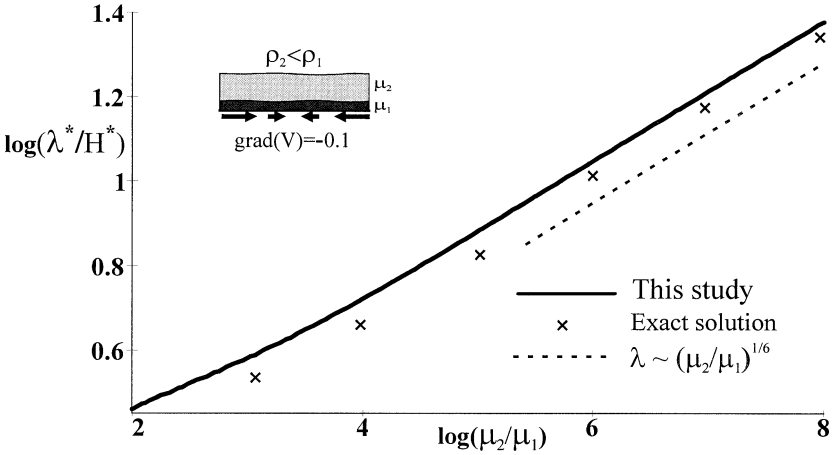

Figure 8. Example B. The dominant wavelength versus viscosity ratio for basal-driven compression with a constant gradient in boundary velocity. Line $\lambda \sim \sqrt[6]{\mu_2/\mu_1}$ illustrates the asymptotic behaviour. The scaling factor for the dimensionless velocity gradient is $(\rho^* g H^*/\mu^*)$ $(h_1/H=0.1,\ \rho_2=0.8\rho_1,\ a_z=0.1)$.

The results of applying the pure SS approach (after Medvedev 1993) and the model of Ellis *et al.* (1995) reformulated for a stable bottom boundary, $V_z=0$, were compared with the results from the ETSA (Fig. 7). The two low-order approaches result in the same spectra, both of which are defined by a velocity gradient V^* and are independent of wavelength.

The behaviour of the dominant wavelength for different viscosity ratios calculated using the ETSA is shown in Fig. 8. It compares well with results of the linear analysis of the full equations ('exact solution').

6 EXAMPLE C: LATERAL EXTENSION OR COMPRESSION OF A LITHOSPHERE BOUNDED BY A LOW-VISCOSITY SUBSTRATE (THE PS CASE)

Consider two layers (e.g. crustal and subcrustal lithosphere) of constant density and viscosity. The non-material lower surface S_1 is the compensation level with the compensation pressure P_c and zero shear stresses constant in time and space. Even though it is constant in time, the vertical velocity across this surface is not necessarily zero. The upper surface S_2 is stress-free:

$$\begin{aligned} &T_x|_{S_1}=0\,, \qquad T_x|_{S_2}=0\,;\\ &T_z|_{S_1}=P_c\,, \qquad T_z|_{S_2}=0\,; \end{aligned} \tag{66}$$

therefore,

$$\overline{T_x}=R_x=0\,, \qquad \overline{T_z}=P_c\,. \tag{67}$$

These boundary conditions can be applied if the upper layer is much more competent than the lower layer ($\mu_2 \gg \mu_1$) (Ranalli 1994; Burov & Diament 1995). The key unknown functions are

$$V_x(x)=v_x(x,z)|_{S_1}\,, \quad V_z(x)=v_z(x,z)|_{S_1}\,, \quad S_1(x)\,, \qquad S_2(x)\,. \tag{68}$$

Partitioning of the vertical boundary conditions is defined by eqs (14):

$$R_z=a_z(\overline{\rho}-P_c)-\overline{\rho}\,, \quad \overline{\Delta T_z}=\varepsilon^{-2}(P_c-\overline{\rho})\,. \tag{69}$$

Substitution of boundary conditions and partitioning into eqs (11)–(12) gives

$$2\,\frac{\partial \overline{\tau_{xx}}}{\partial x}+a_z\,\frac{\partial}{\partial x}\,[H(P_c-\overline{\rho})]-\rho_2 H\,\frac{\partial S_2}{\partial x}+\Delta_\rho h_1\,\frac{\partial S_*}{\partial x}=0\,, \tag{70}$$

$$\frac{\partial^2}{\partial x^2}\,[2\overline{z_c\tau_{xx}}+\overline{M_\rho}-\overline{\rho}\cdot\overline{z_c}+a_z\overline{z_c}(\overline{\rho}-P_c)]+\frac{\partial}{\partial x}\left[(2\overline{\tau_{xx}}+a_z H(\overline{\rho}-P_c)+\overline{\rho}-\overline{\rho}H)\,\frac{\partial w}{\partial x}\right]=\frac{1}{\varepsilon^2}\,(\overline{\rho}-P_c)\,, \tag{71}$$

where the horizontal viscous stress is

$$\overline{\tau_{xx}}=2\left[(\overline{\mu}+\overline{F_{xx}})\,\frac{\partial V_x}{\partial x}-(4\overline{G_{x*}}-2\overline{F_{x*}})\,\frac{\partial^2 V_x}{\partial x^2}-(4\overline{G_{**}}-\overline{F_{**}})\,\frac{\partial^3 V_x}{\partial x^3}+\overline{J_x}\,\frac{\partial V_z}{\partial x}-\overline{J_*}\,\frac{\partial^2 V_z}{\partial x^2}-\overline{Q_{xx}}-(a_z-1)\left(\overline{E_x}\,\frac{\partial \overline{\rho}}{\partial x}-\overline{E_*}\,\frac{\partial^2 \overline{\rho}}{\partial x^2}\right)\right]. \tag{72}$$

This expression is similar to that for the averaged moment of the horizontal viscous stress:

$$\overline{z_c \cdot \tau_{xx}} = 2\left[(\overline{z_c \mu} + \overline{z_c F_{xx}}) \frac{\partial V_x}{\partial x} - \ldots (\text{other terms}) \right]. \tag{73}$$

The evaluation of coefficients presented in Appendix A shows that the only terms having a singularity due to the viscosity contrast in this case are those referred to E. Hence the position of the reference surface w can be defined for several purposes; for example, to make the system easier to manipulate ($w = S_1$) or to drop the singular terms from the vertical force balance [by putting $w = (S_2 + S_3)/2$]. Alternatively, the order of the vertical force balance can be lowered by putting w as the solution of the equation

$$\overline{z_c F_*} - 4\overline{z_c G_{**}} = 0, \tag{74}$$

which is the coefficient for the highest-order derivative of unknown key functions in the vertical force balance ($\partial^5 V_x / \partial x^5$).

The velocity field for $z < S_*$ is

$$v_x = V_x - \frac{3}{2}\varepsilon^2 (z - S_1)^2 \cdot \frac{\partial^2 V_x}{\partial x^2} - \varepsilon^2 (z - S_1) \frac{\partial V_z}{\partial x} - \varepsilon^2 (a_z - 1) \frac{(z - S_1)^2}{2\mu_1} \frac{\partial \overline{\rho}}{\partial x}, \tag{75}$$

and for $z > S_*$ is

$$v_x = V_x - \varepsilon^2 \left[\left(\frac{3}{2}(z - S_1)^2 + 4h_1 (z - S_*) \frac{\Delta_\mu}{\mu_2} \right) \frac{\partial^2 V_x}{\partial x^2} + (z - S_1) \frac{\partial V_z}{\partial x} \right]$$

$$+ \varepsilon^2 (z - S_*)^2 \frac{\Delta_\rho}{2\mu_2} \cdot \frac{\partial S_*}{\partial x} - \varepsilon^2 (a_z - 1) \left(\frac{h_1^2}{2\mu_1} + \frac{h_1 (z - S_*)}{\mu_2} + \frac{(z - S_*)^2}{2\mu_2} \right) \frac{\partial \overline{\rho}}{\partial x}. \tag{76}$$

The combination of kinematic relations eqs (21)–(23) can be integrated here in the form

$$\frac{\partial S_m}{\partial t} + \frac{\partial}{\partial x} \int_{S_1}^{S_m} v_x(x, z) dz = V_z \tag{77}$$

for material boundaries ($S_m = \{S_*, S_2\}$). Integrating the horizontal velocity within the limits of S_1 and the corresponding surface yields equations describing the evolution of the material surfaces:

$$\frac{\partial S_*}{\partial t} + \frac{\partial}{\partial x} \left[V_x h_1 - \frac{\varepsilon^2 h_1^3}{2} \frac{\partial^2 V_x}{\partial x^2} - \frac{\varepsilon^2 h_1^2}{2} \frac{\partial V_z}{\partial x} - (a_z - 1) \frac{\varepsilon^2 h_1^3}{6\mu_1} \cdot \frac{\partial \overline{\rho}}{\partial x} \right] = V_z, \tag{78}$$

$$\frac{\partial S_2}{\partial t} + \frac{\partial}{\partial x}(V_x H) - \varepsilon^2 \frac{\partial}{\partial x} \left[\left(\frac{H^3}{2} + 2h_2^2 h_1 \left(\frac{\mu_1}{\mu_2} - 1 \right) \right) \frac{\partial^2 V_x}{\partial x^2} + \frac{H^2}{2} \cdot \frac{\partial V_z}{\partial x} + \frac{\Delta_\rho h_2^3}{6\mu_2} \cdot \frac{\partial S_*}{\partial x} - (a_z - 1) \left(\frac{H^3}{6\mu_1} - \frac{\delta_\mu}{6\mu_2} (3h_1 h_2^2 + h_2^3) \right) \frac{\partial \overline{\rho}}{\partial x} \right] = V_z. \tag{79}$$

6.1 Simple cases

6.1.1 The PS approach

Neglecting ε terms in the expression for the horizontal velocity of the upper layer ($z > S_*$, eq. 76) results in

$$v_x(x, z) \approx V_x(x). \tag{80}$$

Neglecting the same order terms from the vertical force balance eq. (71) gives the Airy isostasy condition

$$P_c = \rho_1 h_1 + \rho_2 h_2. \tag{81}$$

Algebra gives

$$\frac{\partial}{\partial x}(R_z H + \overline{\overline{\rho}}) = -\Delta_\rho h_2 \cdot \frac{\partial h_1}{\partial x} = -\rho_2 (1 - \rho_2/\rho_1) h_2 \frac{\partial h_2}{\partial x}. \tag{82}$$

Substituting isostasy into the horizontal force balance eq. (70) and neglecting all ε terms yields

$$4 \frac{\partial}{\partial x} \left(\overline{\mu} \frac{\partial V_x}{\partial x} \right) = \frac{\rho_2 (1 - \rho_2/\rho_1)}{2} \frac{\partial h_2^2}{\partial x}. \tag{83}$$

Normalization of both $\overline{\mu}$ and the right-hand part of eq. (83) by H gives the governing equation presented in England & McKenzie (1983).

England & McKenzie (1983) investigated this case using a viscous fluid with a power-law temperature dependence. Estimation of $\overline{\mu}$ can be performed by the technique suggested by England & McKenzie (1982, Appendix A) or by England (1983), which was supported by analytical investigations by Sonder & England (1986). The rheological settings applied in our Example C (two layers with constant viscosities) are not the power-law creep considered by England & McKenzie (1983). However, both cases share the property of the averaged viscosity depending on the horizontal coordinate.

6.1.2 The bending equation

Consider the development of a thin sheet subject to a deviatoric horizontal stress, σ, which is constant inside the layers. The vertical distribution of the deviatoric stress allows pure shear deformations in the system, thus $\sigma_1/\mu_1=\sigma_2/\mu_2=\sigma/\mu$. In the case of perfectly plane boundaries, the unperturbed stress balance in the horizontal plane gives

$$2\mu\,\frac{\partial v_x}{\partial x}-P=\sigma+\sigma_\rho\,, \tag{84}$$

where σ_ρ expresses the lithostatic stress, which is eliminated after substitution of pressure from the vertical stress balance:

$$P=-\sigma_\rho+2\mu\,\frac{\partial v_z}{\partial z}=-\sigma_\rho-2\mu\,\frac{\partial v_x}{\partial x}\,. \tag{85}$$

The unperturbed flow is described by

$$\begin{aligned} &v_x(x,z)=V_x(x)\,, && \frac{\partial V_x}{\partial x}=-\frac{\overline{\sigma}}{4\overline{\mu}}=\text{const}\,, && V_z=\frac{P_\text{c}}{\rho_1}\cdot\frac{\overline{\sigma}}{4\overline{\mu}}=\text{const}\,,\\ &h_2(t)=h_{02}\exp\left(\frac{\overline{\sigma}}{4\overline{\mu}}\,t\right), && h_1(t)=\frac{P_\text{c}-\rho_2 h_2}{\rho_1}\,, && P_\text{c}=\rho_1 h_{01}+\rho_2 h_{02}\,, \end{aligned} \tag{86}$$

where h_{01} and h_{02} are the initial thicknesses of the layers.

The small perturbations of mean flow with long wavelength are assumed not to change the thickness of the competent (upper) layer: $h_2'=0$, and therefore $h_1'=S_*'=S_2'$ (hereafter in this section, primes indicate the perturbed flow parameters). This assumption is common when considering folding and is valid as long as $\mu_2\gg\mu_1$ (Fletcher 1977). These assumptions allow us to linearize the equations, keep only the lowermost derivatives of unknown functions, and neglect insignificant terms due to the condition $\mu_1\ll\mu_2$. The subtraction of eq. (78) from eq. (79) ($a_z=1$) after simplification gives

$$0=\frac{\partial(S_2'-S_1')}{\partial t}=h_2\,\frac{\partial V_x'}{\partial x}-\varepsilon^2\,\frac{H^2-h_1^2}{2}\cdot\frac{\partial^2 V_z'}{\partial x^2}-\frac{\Delta_\rho h_2^3}{6\mu_2}\cdot\frac{\partial^2 S_*'}{\partial x^2}\,. \tag{87}$$

Then, the perturbed horizontal velocity can be expressed as

$$\frac{\partial V_x'}{\partial x}=\varepsilon^2(h_2/2+h_1)\,\frac{\partial^2 V_z'}{\partial x^2}-\frac{\Delta_\rho h_2^2}{6\mu_2}\cdot\frac{\partial^2 S_*'}{\partial x^2}\,. \tag{88}$$

Kinematic eq. (78) gives

$$V_z'=\frac{\partial S_*'}{\partial t}+V_x\,\frac{\partial S_*'}{\partial x}+h_1'\,\frac{\partial V_x}{\partial x}+h_1\,\frac{\partial V_x'}{\partial x}=\frac{dS_*'}{dt}-h_1'\,\frac{\sigma}{4\mu}\,. \tag{89}$$

The vertical force balance eq. (71) can be simplified using the assumptions and form of eq. (25), and after substitution of the coefficients (Appendix A, $w=S_1$), simplification and linearization can be rewritten as

$$\varepsilon^2\,\frac{\partial^2}{\partial x^2}\left[\mu_2(2h_2^2+4h_1h_2)\,\frac{\partial V_x'}{\partial x}+h_1'\overline{\sigma}-\frac{4\varepsilon^2\mu_2}{3}\,(h_2^3+3h_1h_2H)\,\frac{\partial^2 V_z}{\partial x^2}\right]=\rho_1 h_1'\,. \tag{90}$$

Here we use the condition $\sigma/\mu \approx \overline{\sigma}/\overline{\mu}$. Substitution of the horizontal velocity from eq. (88) and the vertical velocity from eq. (89) into the vertical force balance eq. (90) gives

$$\varepsilon^4 \frac{\mu_2 h_c^3}{3} \frac{\partial^4}{\partial^4 x}\left(\frac{dS_*'}{dt}\right) + \varepsilon^2 \overline{\sigma} \frac{\partial^2 S_*}{\partial^2 x} = -\rho_1 h_1'. \tag{91}$$

Then, replacement of the material boundary S_* by the non-material marker S [vertical position of rheological boundary, $(dS/dt = \partial S/\partial t)$], rescaling of the horizontal coordinate using the thickness of a thin sheet (setting $\varepsilon = 1$) and changing the right-hand side to the general case leads to the general bending equation (6-181) of Turcotte & Schubert (1982) (eq. 7 in this paper). Note that the simplifications of the derivations in this section preclude finding any characteristic wavelengths using eq. (91). To investigate characteristic behaviour, the general bending equation should be specified with an external flow influence (Turcotte & Schubert 1982, eq. 6-189; Ramberg 1970a). With the boundary conditions employed in this section, the characteristic behaviour can be investigated with the full ETSA system of equations (70)–(73), as is demonstrated in the next section.

6.2 Buckling and gravity instability

Let us investigate the problem outlined in Section 6.1 with a mean flow described by eqs (84)–(86) and a small perturbation in the form of eq. (26). The density contrast Δ_ρ can be of different sign, allowing either stable ($\Delta_\rho \leq 0$) or unstable ($\Delta_\rho > 0$) density stratifications. With $\sigma > 0$, the lateral stress is compressive, while $\sigma < 0$ indicates extension of the thin sheet.

We first investigated gravity instability alone ($\sigma = 0$); Fig. 9 shows how the growth rate depends on the wavelength. The maximum growth rate is poorly defined for long wavelengths (~ 1 per cent), while the growth rate drops significantly for shorter wavelengths. Both the ETSA and the exact analytical solution demonstrate this behaviour. Application of the PS approach gives an entirely impractical mean growth rate for almost all wavelengths.

Application of compressional (Fig. 10) or extensional lateral stresses to the system leads to more clearly defined dominant wavelengths. Fig. 11 compares the results of this section with analogue and analytical investigations presented in Ramberg & Stephansson (1964) and Ramberg (1970a,b).

An additional investigation shows that the results are not strongly influenced by the partitioning coefficient a_z in the limits $0 \leq a_z \leq 1$. The dependence of spectra on partitioning is recognizable only for wavelengths shorter than $2H^*$, and more realistic results can be obtained with $a_z \sim 1$.

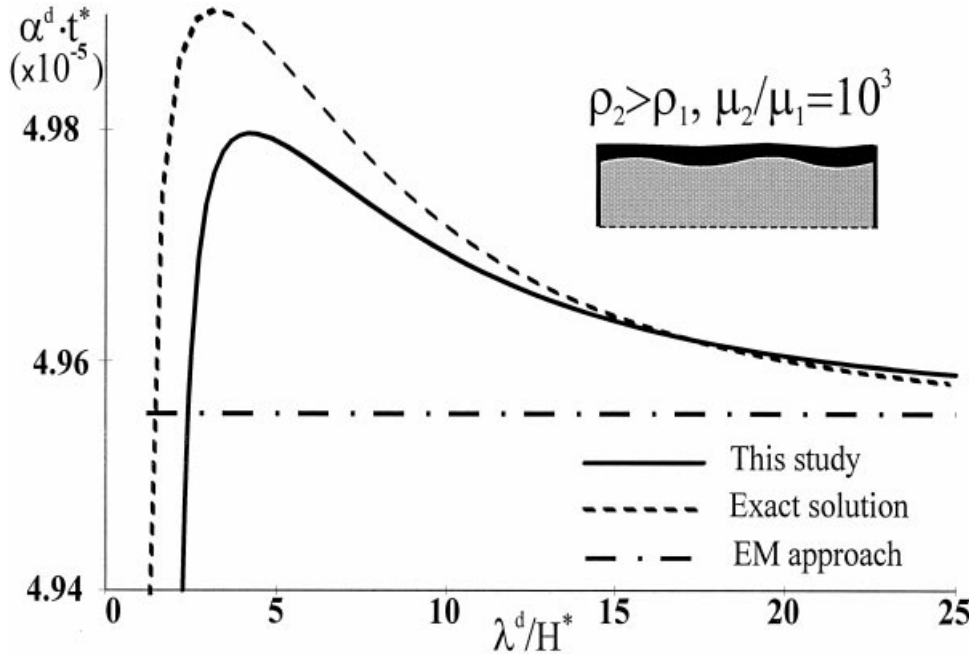

Figure 9. Example C. Instability in two-layer systems with inverted density. The bottom boundary is the non-material level of compensation. The dominant wavelength is poorly distinguished (~ 1 per cent) for this case; the growth rate α tends to $-\infty$ for short wavelengths. The PS approach shows no changes over the range of wavelengths considered ($h_2/H = 0.1$, $\rho_2 = 2\rho_1$, $a_z = 1$).

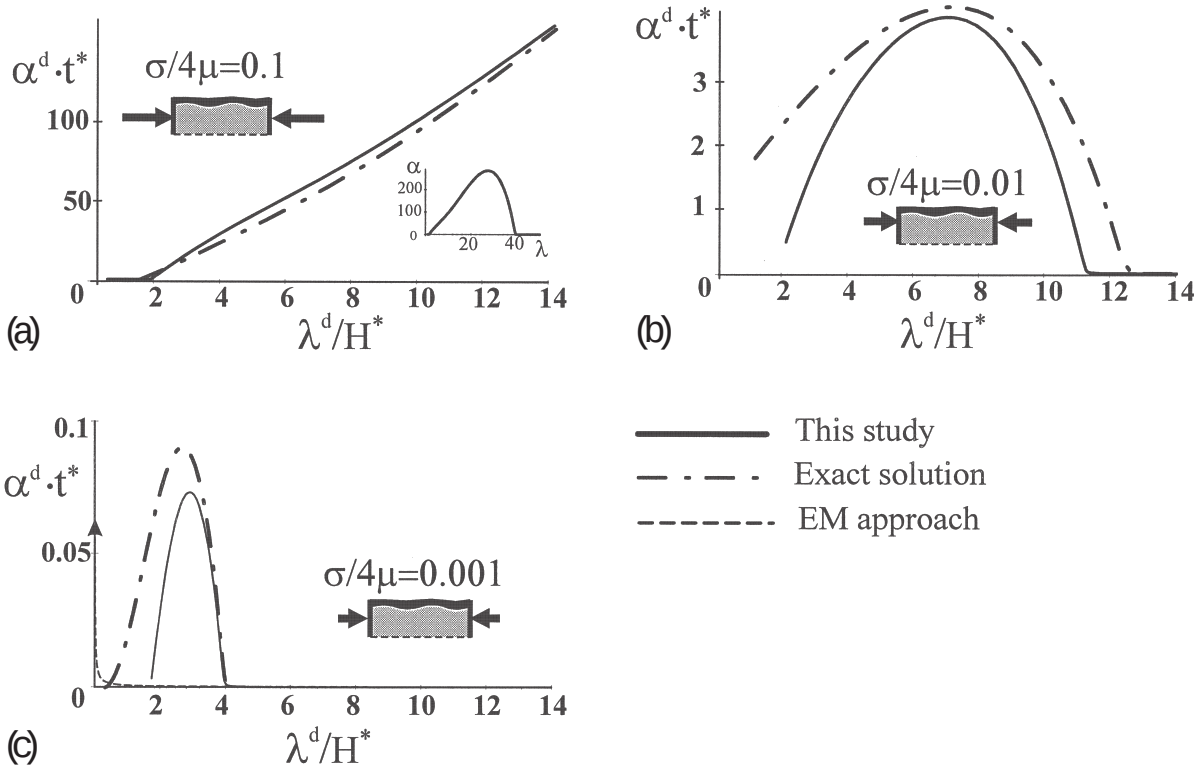

Figure 10. Example C. Interaction of a gravity instability and folding for a two-layer system with inverted density due to lateral compression with different rates. The gravity instability is not recognizable for $\sigma/4\mu > 10^{-4}$. The dominant wavelength and corresponding growth rate increase with increasing applied force. Both the PS approach and the ETSA demonstrate the same tendency at long wavelengths. However, the PS approach has no dominant wavelengths and shows inappropriate behaviour approaching short wavelengths. The dimensionless uniform strain rate of mean flow is $\sigma/4\mu = -(\partial V_x^0/\partial x)$ with scaling factor $(\rho^* g H^*/\mu^*)$. Note that wavelengths are scaled to the thickness of the whole system. To rescale the wavelength for upper-layer thickness, it should be multiplied by a factor of 10 ($h_2/H = 0.1$, $\rho_2 = 2\rho_1$, $\mu_2/\mu_1 = 10^3$, $a_z = 1$).

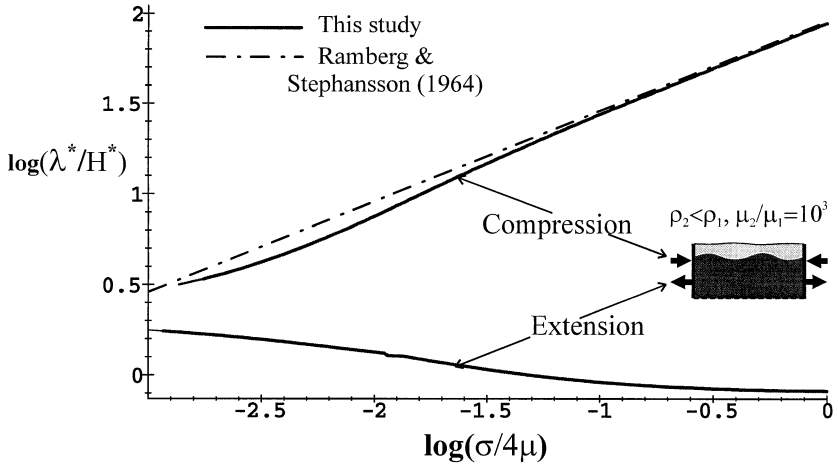

Figure 11. Example C. The dominant wavelengths for the two-layer system due to different magnitudes of lateral compression and extension. There is no density inversion in this case ($\rho_2 = 0.8\rho_1$). The curve for compression satisfies the asymptotic behaviour predicted by Ramberg & Stephansson (1964) well. The scaling factor for the dimensionless parameter of this example ($\sigma/4\mu$) is $(\rho^* g H^*/\mu^*)$ ($h_2/H = 0.1$, $\mu_2/\mu_1 = 10^3$, $a_z = 0$).

7 CONCLUSIONS

7.1 Partitioning coefficient

The analytical treatment of MP99 leaves the vertical boundary partitioning coefficient a_z as a free parameter in the ETSA. This parameter represents the relation between approximate profiles of stress functions and their integrated correction. MP99 demonstrated that the value of a_z gives preference to satisfying certain boundary conditions at a low level of approximation [i.e. by the approximate stress profile, eq. (8), which is able to satisfy only one boundary condition].

Our tests show that the influence of the partitioning becomes insignificant at wavelengths longer than about double the characteristic wavelength. Thus, investigations of the influence of partitioning are limited by intermediate (near-characteristic) wavelengths.

Example C (the PS case) shows a very low dependence of solutions on the choice of the partitioning coefficient unless $0 \leq a_z < 1$. The need for solutions to be realistic over a wide range of wavelengths defines the preferential choice of $a_z \sim 1$ by investigating wavelengths shorter than $2H^*$.

When the bottom boundary is subjected to external shear (the SS case, example B), our tests show that preference should be given to the external horizontal boundary which is closer to the most intense rheological gradients within the model domain. In the few examples we have studied, this approach resulted in extremely accurate asymptotic solutions.

The ETSA was also tested with free-slip along the bottom boundary. All cases were found to be strongly dependent on the partitioning and we did not identify the most appropriate partitioning rule because the technique we applied in example B failed to improve the solutions. Rayleigh–Taylor instability spectra for the case of a free-slip boundary condition compare well with the exact solution using negative values of the partitioning coefficient: $-1 \leq a_z < 0$. The most appropriate choice for the partitioning coefficient for this case needs further work.

7.2 Results of experiments

Testing problems were investigated on the basis of single- and two-layer models of Newtonian viscous materials. Linear analyses compare well with exact analytical solutions over a wide range of wavelengths for the modelling of isostatic adjustment, Rayleigh–Taylor instabilities and buckling due to compression and extension. The examples show the following.

(1) The new ETSA generalizes the most popular existing thin-sheet approximations. Whereas existing approaches only allow particular types of boundary conditions, the new model allows stipulation of all likely geodynamic boundary conditions. It was shown that the previous generation of thin-sheet approximations could be derived by simplification of the ETSA under each of their restricted boundary conditions.

(2) Comparison of exact 2-D solutions with our results shows the surprisingly high accuracy of the ETSA. Accurate instability spectra defined by linear analyses were obtained by our long-wavelength approximation, even at short wavelengths.

(3) The ETSA can be applied to geodynamic problems that cannot be described by previous thin-sheet approximations. Only buckling could be handled by the FP approach. The development of other mechanical instabilities was not possible with any of the previous generation of thin-sheet models, even where the competence (viscosity) contrast was high and the dominant wavelengths were much longer than the thickness of the thin sheet.

(4) The examples presented here are 2-D; however, the formulation and final equations of the ETSA are 3-D (3-D tests are in preparation). However, even the 2-D model shows great advantages for investigations of the evolution of 2-D structures.

The results of this work show that the new extended thin-sheet approximation is a powerful tool for realistic modelling of complicated 2- and 3-D geodynamic structures.

ACKNOWLEDGMENTS

Prof. C. J. Talbot is thanked for improving the structure and presentation of this work. The authors thank D. McKenzie, H. Zeyen, A. Poliakov and two anonymous reviewers for helpful discussions and suggestions that improved the manuscript. This work was supported by an Uppsala University PhD Fellowship to SM.

REFERENCES

Bird, P., 1991. Lateral extrusion of lower crust from under high topography, in the isostatic limit, *J. geophys. Res.,* **96,** 10 275–10 286.

Buck, W.R., 1991. Modes of continental lithospheric extension, *J. geophys. Res.,* **96,** 20 161–20 178.

Buck, W.R. & Sokoutis, D., 1994. Analogue model of gravitational collapse and surface extension during continental convergence, *Nature,* **369,** 737–740.

Burov, E.B. & Diament, M., 1992. Flexure of the continental lithosphere with multilayered rheology, *Geophys. J. Int.,* **109,** 449–468.

Burov, E.B. & Diament, M., 1995. The effective elastic thickness (T_e) of continental lithosphere: what does it really mean?, *J. geophys. Res.,* **100,** 3905–3927.

Ellis, S., Fullsack, P. & Beaumont, C., 1995. Oblique convergence of the crust driven by basal forcing: implication for length-scales of deformation and strain partitioning in orogens, *Geophys. J. Int.,* **120,** 24–44.

England, P., 1983. Constraints on extension of continental lithosphere, *J. geophys. Res.,* **88,** 1145–1152.

England, P. & McKenzie, D., 1982. A thin viscous sheet model for continental deformation, *Geophys. J. R. astr. Soc.,* **70,** 295–321.

England, P. & McKenzie, D., 1983. Correction to: a thin viscous sheet model for continental deformation, *Geophys. J. R. astr. Soc.,* **73,** 523–532.

Fletcher, R.S., 1977. The shape of single layer folds at small but finite amplitude, *Tectonophysics,* **39,** 593–606.

Kaufman, P.S. & Royden, L.H., 1994. Lower crustal flow in extensional settings: constraints from the Halloran Hills

region, eastern Mojave Desert, California, *J. geophys. Res.,* **99,** 15 723–15 739.
Lobkovsky, L.I. & Kerchman, V.I., 1991. A two-level concept of plate tectonics: application to geodynamics, *Tectonophysics,* **199,** 343–374.
Medvedev S.E., 1993. Computer simulation of sedimentary cover evolution, in *Computerized Basin Analysis: the Prognosis of Energy and Mineral Resources,* pp. 1–10, eds Harff, J. & Merriam, D.F., Plenum, New York.
Medvedev S.E. & Podladchikov, Yu.Yu., 1999. New extended thin-sheet approximation for geodynamic applications—I. Model formulation, *Geophys. J. Int.,* **136,** 567–585 (this issue).
Ramberg, H., 1968a. Instability of layered system in the field of gravity, 1, *Phys. Earth planet. Inter.,* **1,** 427–447.
Ramberg, H., 1968b. Instability of layered system in the field of gravity, 2, *Phys. Earth planet. Inter.,* **1,** 448–474.
Ramberg, H., 1970a. Folding of laterally compressed multilayers in the field of gravity, 1, *Phys. Earth planet. Inter.,* **2,** 203–232.
Ramberg, H., 1970b. Folding of laterally compressed multilayers in the field of gravity, 2, Numerical examples, *Phys. Earth planet. Inter.,* **4,** 83–120.
Ramberg, H., 1981. *Gravity, Deformation and the Earth's Crust,* 2nd edn, Academic Press, New York.
Ramberg, H. & Stephansson, O., 1964. Compression of floating elastic and viscous plates affected by gravity, a basis for discussing crustal buckling, *Tectonophysics,* **1,** 101–120
Ranalli, G., 1994. Nonlinear flexure and equivalent mechanical thickness of the lithosphere, *Tectonophysics,* **240,** 107–114.
Royden, L., 1996. Coupling and decoupling of crust and mantle in convergent orogens: implications for strain partitioning in the crust, *J. geophys. Res.,* **101,** 17 679–17 705.
Sonder, L.J. & England, P., 1986. Vertical averages of rheology of the continental lithosphere: relation to thin sheet parameters, *Earth planet. Sci. Lett.,* **77,** 81–90.
Talbot, C.J., Medvedev, S., Alavi, M., Shahrivar, H. & Heidari, E, 1998. Salt extrusion rates at Kuh-e-Jahani, Iran: June 1994 to November 1996, in preparation.
Turcotte, D.L. & Schubert, G., 1982. *Geodynamics—Applications of Continuum Physics to Geological Problems,* John Willey, New York.
Wdowinski, S., O'Connell, R.J. & England, P., 1989. A continuum model of continental deformation above subduction zones: application to the Andes and the Aegean, *J. geophys. Res.,* **94,** 10 331–10 346.
Whitehead, J.A., 1988. Fluid models of geological hotspots, *Ann. Rev. Fluid Mech.,* **20,** 61–87.
Zanemonetz, V.B., Mikhajlov, V.O. & Myasnikov, V.P., 1976. Mechanical model of block folding formation, *Phys. Solid Earth,* **12,** 631–635.

APPENDIX A: EVALUATION OF INTEGRATED FUNCTIONS FOR TWO-LAYER SYSTEMS (EXAMPLES B AND C)

The momentum integration auxiliary function is introduced by

$$\overline{z_c}^{(k)} = \int_{S_1}^{S_2} z_c \left(\underbrace{\int \cdots \int}_{k} dz \ldots dz \right) dz \,. \tag{A1}$$

Therefore,

$$\begin{aligned} &\overline{z_c}^{(0)} = \overline{z_c} = \frac{H^2}{2} - h_w H \,, \qquad \overline{z_c}^{(1)} = \frac{H^3}{3} - h_w \frac{H^2}{2} \,, \\ &\overline{z_c}^{(2)} = \frac{H^4}{8} - h_w \frac{H^3}{6} \,, \qquad \overline{z_c}^{(3)} = \frac{H^5}{15} - h_w \frac{H^4}{12} \,. \end{aligned} \tag{A2}$$

The heterogeneity functions for the case of two layers are

$$\delta_\mu = \left(\frac{\mu_2}{\mu_1} - 1 \right) , \qquad M_\mu = \left(\frac{h_2^2}{2} - h_* h_2 \right) \delta_\mu \,, \tag{A3}$$

where $h_w = (w - S_1)$, $h_* = (w - S_*)$. The other integrated functions of this case are presented in a form which distinguishes them from the single-layer system. Setting all differences (Δ_ρ and Δ_μ) and heterogeneity functions (δ_μ and M_μ) equal to 0 and $\rho_1 = \rho$, $\mu_2 = \mu$ leads to integrated functions for the single-layer system. The averaged rheological functions applied in the force balance are

$$\begin{aligned} &\overline{\rho} = \rho_1 H + \Delta_\rho h_2 \,, && \overline{\mu} = \mu_2 H - \Delta_\mu h_1 \,, \\ &\overline{\overline{\rho}} = \rho_1 H^2/2 + \Delta_\rho h_2^2/2 \,, && \overline{\overline{\mu}} = (\mu_2 H^2 - \Delta_\mu h_1^2)/2 \,, \\ &\overline{M_\rho} = \rho_1 \overline{z_c}^{(1)} + \Delta_\rho \left(\frac{h_2^3}{3} - h_* \frac{h_2^2}{2} \right) , && \overline{z_c \cdot \mu} = \mu_2 \overline{z_c} - \Delta_\mu \left(\frac{h_1^2}{2} - h_w h_1 \right) . \end{aligned} \tag{A4}$$

The evaluation of integrated coefficients for horizontal force balance is presented in Table A1. The evaluation of integrated coefficients for vertical force balance is presented in Table A2. Coefficients of $\overline{\overline{D}}$ type are very large after the triple derivations and integrations. Hence evaluation of these coefficients is presented in a separate table, Table A3.

Table A1. Integrated functions for horizontal force balance.

$$
\begin{aligned}
\overline{D_*} &= \varepsilon(H^2/2+\delta_\mu h_1 h_2)\\
\overline{D_x} &= \varepsilon\left(-H\cdot\frac{\partial S_1}{\partial x}+\delta_\mu h_2\,\frac{\partial h_1}{\partial x}\right)\\
\overline{E_*} &= \varepsilon^2\left(H^3/6+\delta_\mu h_1^2 h_2/2\right)\\
\overline{E_x} &= \varepsilon^2\left(-\frac{\partial S_1}{\partial x}\,H^2/2+\delta_\mu h_1 h_2\,\frac{\partial h_1}{\partial x_i}\right)\\
\overline{F_{xx}} &= \varepsilon^2\left(\overline{\mu}\left(\frac{\partial S_1}{\partial x}\right)^2+\frac{\partial^2 S_1}{\partial x^2}\,(\Delta_\mu h_1^2/2-\mu_2 H^2/2)\right)\\
\overline{F_{x*}} &= \varepsilon^2\,\frac{\partial S_1}{\partial x}\,(\Delta_\mu h_1^2/2-\mu_2 H^2/2)\\
\overline{F_{**}} &= \varepsilon^2(\mu_2 H^3-\Delta_\mu h_1^3)/6\\
\overline{G_{xx}} &= 0\\
\overline{G_{*x}} &= 0\\
\overline{G_{x*}} &= \varepsilon^2\left[\Delta_\mu\left(\frac{\partial S_*}{\partial x}\,h_1 h_2-\frac{\partial h_1}{\partial x}\,h_2^2/2\right)-\mu_2\,\frac{\partial S_1}{\partial x}\,H^2/2\right]\\
\overline{G_{**}} &= \varepsilon^2(\mu_2 H^3/6-\Delta_\mu(h_1^3/6+h_1 h_2^2/2))\\
\overline{J_x} &= \varepsilon^2\overline{\mu}\,\frac{\partial S_1}{\partial x}\\
\overline{J_*} &= \varepsilon^2(\mu_2 H^2/2-\Delta_\mu h_1^2/2)\\
\overline{Q_{xx}} &= \varepsilon^2\rho_1\left[\left(\frac{\partial S_1}{\partial x}\right)^2\frac{H^2}{2}-\frac{\partial^2 S_1}{\partial x^2}\,\frac{H^3}{6}-\delta_\mu h_2\,\frac{\partial}{\partial x}\left(\frac{\partial S_1}{\partial x}\,\frac{h_1^2}{2}\right)\right]+\varepsilon^2\Delta_\rho\left[\left(\frac{\partial S_*}{\partial x}\right)^2\frac{h_2^2}{2}-\frac{\partial^2 S_*}{\partial x^2}\,\frac{h_2^3}{6}\right]
\end{aligned}
$$

Table A2. Integrated functions for vertical force balance.

$$
\begin{aligned}
\overline{z_c D_*} &= \varepsilon(\overline{z_c}^{(1)}+M_\mu h_1)\\
\overline{z_c D_x} &= \varepsilon\left(M_\mu\,\frac{\partial h_1}{\partial x}-\overline{z_c}\,\frac{\partial S_1}{\partial x}\right)\\
\overline{z_c E_*} &= \varepsilon^2(\overline{z_c}^{(2)}+M_\mu h_1^2/2)\\
\overline{z_c E_x} &= \varepsilon^2\left(M_\mu h_1\,\frac{\partial h_1}{\partial x}-\overline{z_c}^{(1)}\,\frac{\partial S_1}{\partial x}\right)\\
\overline{z_c F_{xx}} &= \varepsilon^2\left[\left(\frac{\partial S_1}{\partial x}\right)^2\overline{z_c\mu}+\frac{\partial^2 S_1}{\partial x^2}\left(\mu_2\overline{z_c}^{(1)}-\Delta_\mu\left(\frac{h_1^3}{3}-h_w\,\frac{h_1^2}{2}\right)\right)\right]\\
\overline{z_c F_{x*}} &= \varepsilon^2\,\frac{\partial S_1}{\partial x}\left[\Delta_\mu\left(\frac{h_1^3}{3}-h_w\,\frac{h_1^2}{2}\right)-\mu_2\overline{z_c}^{(1)}\right]\\
\overline{z_c F_{**}} &= \varepsilon^2\left[\mu_2\overline{z_c}^{(2)}-\Delta_\mu\left(\frac{h_1^4}{8}-h_w\,\frac{h_1^3}{6}\right)\right]\\
\overline{z_c G_{xx}} &= 0\\
\overline{z_c G_{*x}} &= 0\\
\overline{z_c G_{x*}} &= -\varepsilon^2\mu_2\overline{z_c}^{(1)}\,\frac{\partial S_1}{\partial x}+\varepsilon^2\Delta_\mu\left[\frac{\partial S_*}{\partial x}\left(h_* h_1 h_2-\frac{h_1 h_2^2}{2}\right)+\frac{\partial h_1}{\partial x}\left(\frac{h_2^3}{3}-\frac{h_* h_2^2}{2}\right)+\frac{\partial S_1}{\partial x}\left(\frac{h_w h_1^2}{2}-\frac{h_1^3}{3}\right)\right]\\
\overline{z_c G_{**}} &= \varepsilon^2\mu_2\overline{z_c}^{(2)}-\varepsilon^2\Delta_\mu\left[\frac{h_1^4}{8}+\frac{h_1 h_2^3}{3}-h_w\left(\frac{h_1^3}{6}+\frac{h_1 h_2^2}{2}\right)\right]\\
\overline{z_c J_x} &= \varepsilon^2\overline{z_c\mu}\,\frac{\partial S_1}{\partial x}\\
\overline{z_c J_*} &= \varepsilon^2\left[\mu_2\overline{z_c}^{(1)}-\Delta_\mu\left(\frac{h_1^3}{3}-h_w\,\frac{h_1^2}{2}\right)\right]\\
\overline{z_c Q_{xx}} &= \varepsilon^2\rho_1\left[\left(\frac{\partial S_1}{\partial x}\right)^2\overline{z_c}^{(1)}-\frac{\partial^2 S_1}{\partial x^2}\,\overline{z_c}^{(2)}-M_\mu\,\frac{\partial}{\partial x}\left(\frac{\partial S_1}{\partial x}h_1\right)\right]+\varepsilon^2\Delta_\rho\left[\left(\frac{\partial S_*}{\partial x}\right)^2\left(\frac{h_2^3}{3}-h_*\,\frac{h_2^2}{2}\right)-\frac{\partial^2 S_*}{\partial x^2}\left(\frac{h_2^4}{8}-h_*\,\frac{h_2^3}{6}\right)\right]
\end{aligned}
$$

Table A3. $\tilde{D}$-related integrated functions.

$$
\begin{aligned}
\overline{\tilde{D}_{xxx}} &= \varepsilon^3\left[-\frac{\partial^3 S_1}{\partial x^3}\cdot\frac{H^3}{6}-\left(\frac{\partial S_1}{\partial x}\right)^3 H+\frac{\partial S_1}{\partial x}\frac{\partial^2 S_1}{\partial x^2}\cdot\frac{3H^2}{2}\right]\\
&\quad+\varepsilon^3\delta_\mu h_2\left[\frac{\partial^3 h_1}{\partial x^3}\frac{h_2^2}{6}+\left(\frac{\partial h_1}{\partial x}\right)^3 h_2-\frac{\partial^3 S_1}{\partial x^3}\frac{h_1 H}{2}+3\frac{\partial S_*}{\partial x}\left(\frac{\partial S_1}{\partial x}\frac{\partial h_1}{\partial x}-\frac{\partial^2 h_1}{\partial x^2}\frac{h_2}{2}\right)+3\frac{\partial^2 S_1}{\partial x^2}\left(\frac{\partial S_1}{\partial x}h_1-\frac{\partial h_1}{\partial x}\frac{h_2}{2}\right)\right]\\
\overline{\tilde{D}_{*xx}} &= \varepsilon^3\left[\left(\frac{\partial S_1}{\partial x}\right)^2\frac{H^2}{2}-\frac{\partial^2 S_1}{\partial x^2}\cdot\frac{H^3}{6}\right]+\varepsilon^3\delta_\mu h_2\left[\left(\frac{\partial S_1}{\partial x}\right)^2 h_1-\frac{\partial^2 S_1}{\partial x^2}\cdot\frac{h_1 H}{2}-\frac{\partial S_1}{\partial x}\frac{\partial h_1}{\partial x}h_2-\left(\frac{\partial h_1}{\partial x}\right)^2\frac{h_2}{2}+\frac{\partial^2 h_1}{\partial x^2}\cdot\frac{h_2^2}{6}\right]\\
\overline{\tilde{D}_{**x}} &= -\varepsilon^3\frac{\partial S_1}{\partial x}\frac{H^3}{6}+\varepsilon^3\delta_\mu h_2\left[\frac{\partial h_1}{\partial x}\frac{h_2^2}{6}-\frac{\partial S_1}{\partial x}\frac{h_1 H}{2}\right]\\
\overline{\tilde{D}_{***}} &= \varepsilon^3\frac{H^4}{24}+\varepsilon^3\delta_\mu h_1 h_2^2\left(\frac{h_2}{6}+\frac{h_1}{4}\right)\\
\overline{z_c\tilde{D}_{xxx}} &= \varepsilon^3\left[\frac{\partial S_1}{\partial x}\frac{\partial^2 S_1}{\partial x^2}\overline{z_c}^{(1)}-\frac{\partial^3 S_1}{\partial x^3}\overline{z_c}^{(2)}-\left(\frac{\partial S_1}{\partial x}\right)^3\overline{z_c}\right]+\varepsilon^3\delta_\mu h_2\left[\frac{\partial^3 h_1}{\partial x^3}\left(\frac{h_2^2}{8}-h_*\frac{h_2}{6}\right)+\left(\frac{\partial h_1}{\partial x}\right)^3\left(\frac{2h_2^2}{3}-h_* h_2\right)-\frac{\partial^3 S_1}{\partial x^3}\left(\frac{h_1^2 h_2^2}{4}+\frac{h_1 h_2^3}{3}-h_*\frac{h_1 h_2 H}{2}\right)\right.\\
&\quad\left.+3\frac{\partial S_*}{\partial x}\left(\frac{\partial S_1}{\partial x}\frac{\partial h_1}{\partial x}\left(\frac{h_2}{2}-h_*\right)-\frac{\partial^2 h_1}{\partial x^2}\left(\frac{h_2^2}{3}-h_*\frac{h_2}{2}\right)\right)+3\frac{\partial^2 S_1}{\partial x^2}\left(\frac{\partial S_1}{\partial x}h_1\left(\frac{h_2}{2}-h_*\right)-\frac{\partial h_1}{\partial x}\left(\frac{h_2^2}{3}-h_*\frac{h_2}{2}\right)\right)\right]\\
\overline{z_c\tilde{D}_{*xx}} &= \varepsilon^3\left[\left(\frac{\partial S_1}{\partial x}\right)^2\overline{z_c}^{(1)}-\frac{\partial^2 S_1}{\partial x^2}\overline{z_c}^{(2)}\right]+\varepsilon^3\delta_\mu h_2\left[\left(\frac{\partial S_1}{\partial x}\right)^2\left(\frac{h_2}{2}-h_*\right)h_1-\frac{\partial^2 S_1}{\partial x^2}\left(\frac{h_1^2 h_2^2}{4}+\frac{h_1 h_2^3}{3}-h_*\frac{h_1 h_2 H}{2}\right)-\frac{\partial S_1}{\partial x}\frac{\partial h_1}{\partial x}\left(\frac{2h_2^2}{3}-h_* h_2\right)\right.\\
&\quad\left.-\left(\frac{\partial h_1}{\partial x}\right)^2\left(\frac{h_2^2}{3}-h_*\frac{h_2}{2}\right)+\frac{\partial^2 h_1}{\partial x^2}\left(\frac{h_2^2}{8}-h_*\frac{h_2}{6}\right)\right]\\
\overline{z_c\tilde{D}_{**x}} &= \varepsilon^3\overline{z_c}^{(2)}\frac{\partial S_1}{\partial x}+\varepsilon^3\delta_\mu h_2\left[\frac{\partial h_1}{\partial x}\left(\frac{h_2^2}{8}-h_*\frac{h_2}{6}\right)-\frac{\partial S_1}{\partial x}\left(\frac{h_1^2 h_2^2}{4}+\frac{h_1 h_2^3}{3}-h_*\frac{h_1 h_2 H}{2}\right)\right]\\
\overline{z_c\tilde{D}_{***}} &= \varepsilon^3\overline{z_c}^{(3)}+\varepsilon^3\delta_\mu h_1 h_2^2\left[\frac{h_2^2}{8}+\frac{h_1 h_2}{3}-h_*\left(\frac{h_2}{6}+h_1\right)\right]
\end{aligned}
$$